

# LLE Review

## Quarterly Report



January–March 1989

Laboratory for Laser Energetics  
College of Engineering and Applied Science  
University of Rochester  
250 East River Road  
Rochester, New York 14623-1299



# LLE Review

## Quarterly Report

*Editor:* P. W. McKenty  
(716) 275-3865

January–March 1989

---



Laboratory for Laser Energetics  
College of Engineering and Applied Science  
University of Rochester  
250 East River Road  
Rochester, New York 14623-1299

This report was prepared as an account of work conducted by the Laboratory for Laser Energetics and sponsored by Empire State Electric Energy Research Corporation, New York State Energy Research and Development Authority, Ontario Hydro, the University of Rochester, the U.S. Department of Energy, and other United States government agencies.

Neither the above named sponsors, nor any of their employees, makes any warranty, expressed or implied, or assumes any legal liability or responsibility for the accuracy, completeness, or usefulness of any information, apparatus, product, or process disclosed, or represents that its use would not infringe privately owned rights.

Reference herein to any specific commercial product, process, or service by trade name, mark, manufacturer, or otherwise, does not necessarily constitute or imply its endorsement, recommendation, or favoring by the United States Government or any agency thereof or any other sponsor.

Results reported in the LLE Review should not be taken as necessarily final results as they represent active research. The views and opinions of authors expressed herein do not necessarily state or reflect those of any of the above sponsoring entities.

## IN BRIEF

This volume of the LLE Review, covering the period January–March 1989, contains the first part of a two-part series of articles dealing with the OMEGA Upgrade. The two articles in this issue discuss the theoretical and laser design work performed to characterize the basic requirements for the upgrade. In addition, the advanced technology section contains articles discussing a new computer code developed to model x-ray refraction in line-focus geometry and experiments involving the use of time-resolved spectroscopy to diagnose high density in argon implosions. Finally, the activities of the National Laser Users Facility and the GDL and OMEGA laser facilities are summarized.

The following are highlights of the research reports contained in this issue:

- A direct-drive, ignition-scaling implosion facility is necessary to address many key physics issues relevant to the future of inertial confinement fusion (ICF). These key issues are introduced and the requirements (for an upgrade to the present OMEGA system) needed to address them are identified.
- A laser system capable of uniformly targeting 30 kJ of ultraviolet light within a shaped pulse presents several difficult challenges to laser designers. The laser requirements of the OMEGA Upgrade and how they are to be incorporated into existing hardware and space is discussed.

- CASER (combine amplified spontaneous emission with refraction), a new code to model radiation transport in three dimensions through a line-focus plasma, is introduced. Applications to x-ray laser experiments at LLNL and LLE are presented.
- A series of experiments supported by the NLUF, in collaboration with laboratory investigators, studied the implosion of Ar-filled plastic microballoons. The spectroscopic data is presented and the presence of high density is discussed.

# CONTENTS

	<i>Page</i>
IN BRIEF .....	iii
CONTENTS .....	v
Section 1 THE OMEGA UPGRADE .....	61
Part I: Theory and Design .....	61
1.A Direct-Drive, High-Gain, Hydrodynamics Equivalent Experiments Facility .....	66
1.B Laser Design and Performance .....	79
Section 2 ADVANCED TECHNOLOGY DEVELOPMENTS .....	88
2.A CASER—A New Code for Calculating the X-Ray Laser Emission from Line-Focus Plasmas .....	88
2.B Time-Resolved Spectroscopic Measurements of High Density in Ar-Filled Microballoon Implosions .....	99
Section 3 NATIONAL LASER USERS FACILITY NEWS .....	107
Section 4 LASER SYSTEM REPORT .....	109
4.A GDL Facility Report .....	109
4.B OMEGA Facility Report .....	110
PUBLICATIONS AND CONFERENCE PRESENTATIONS	



Sam Letzring, Diagnostic Development Group Leader, is shown adjusting the holographic transmission grating used to temporally shear the laser beam before it passes through the electro-optic phase modulator in the smoothing by spectral dispersion (SSD) scheme, which was recently implemented on the OMEGA laser system.

# **Section 1**

## **THE OMEGA UPGRADE**

### **Part I: Theory and Design**

The objective of the U. S. Inertial Confinement Fusion (ICF) Program is to develop a laboratory microfusion capability for military and energy-production applications. Attaining the objectives of the ICF program depends critically on understanding the physics of thermonuclear ignition and burn. The development of the required ICF physics data base depends to a large extent on the experimental target-implosion programs being carried out on the NOVA laser at Lawrence Livermore National Laboratory (LLNL) and the OMEGA laser at the University of Rochester Laboratory for Laser Energetics (LLE). With an energy capability of 100,000 J, the NOVA laser is the primary laboratory driver for the U.S. ICF program and is being used to carry out x-ray-driven ICF target-implosion experiments. OMEGA, a 4,000-J, uniform-illumination laser, is the primary U.S. facility used to explore the feasibility of the direct-drive approach to ICF. Both of these experimental programs have demonstrated high-density compression of fusion capsules—a key requirement for the eventual success of ICF.

While the current OMEGA experiments are important in addressing many key ICF issues, a higher-energy, direct-drive capability provided by an upgrade of this laser, would achieve sufficient thermonuclear yield to address ignition-scaling issues. These experiments could increase the confidence level associated with the success of a national high-gain laboratory facility. Preliminary design engineering and development and related studies for the upgrade of the OMEGA

facility are currently in progress. In this and the following issue of the LLE Review, we review the present status of the OMEGA Upgrade design engineering and development effort, including a conceptual design of the upgrade.

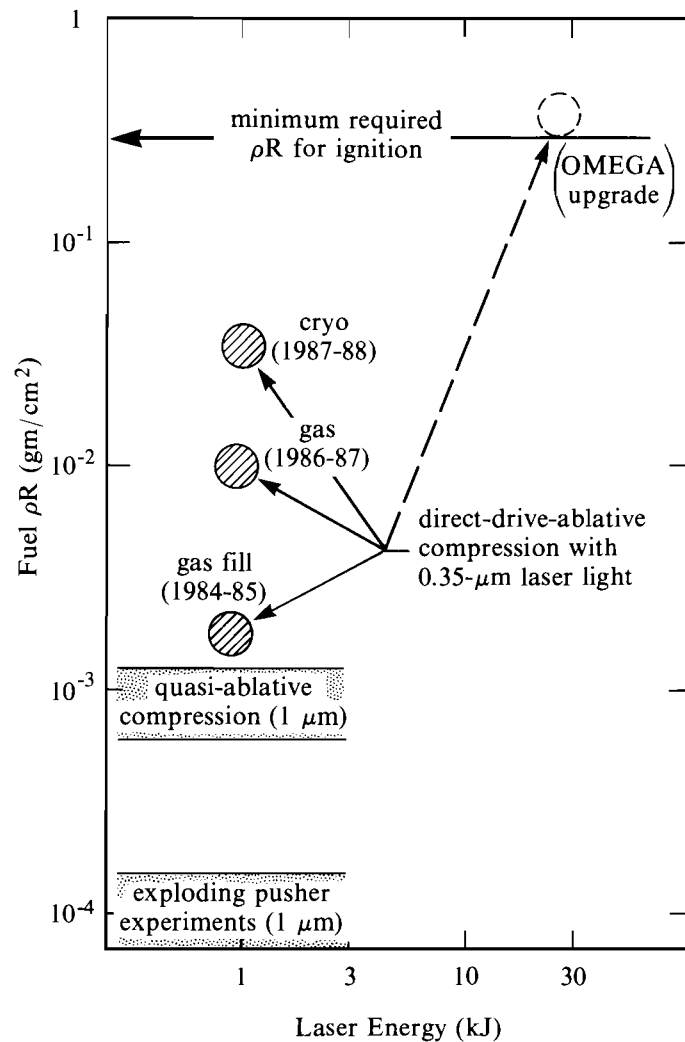
### **Purpose of the Proposed OMEGA Upgrade**

There are two approaches to inertial fusion: indirect (or hohlraum) drive and direct drive. The indirect-drive approach, which involves the conversion of the driver energy into x rays to drive a fuel capsule, is the main-line approach of the U.S. national program and is being pursued at LLNL and the Los Alamos and Sandia National Laboratories. Direct drive involves the direct irradiation of a fuel pellet by energy from the driver (laser or particle beam) and may be energetically more efficient than indirect drive.

The direct-drive approach to short-wavelength laser fusion is not only an alternative approach to inertial fusion, but also an essential tool for obtaining the capsule-physics technical base required to understand critical ICF issues. The next critical issue in ICF to be addressed, after the demonstration of high-density and high-convergence implosions, is the production of a small region of plasma at ignition temperature and density. Ignition refers to the rapid thermonuclear burning of fusion fuel that simultaneously achieves high density and temperature to trigger the reaction. Once ignition occurs, high-energy thermonuclear-reaction products redeposit their energy in cold, unignited thermonuclear fuel surrounding the region and cause a thermonuclear burn wave to propagate. It is the propagation of the burn wave that is responsible for high gain. If the required degree of drive uniformity is achieved, it may be possible with direct drive to achieve high-density target compression and thermonuclear ignition conditions with less laser energy than is required to carry out hohlraum-driven implosions. Achievement of these conditions would strongly support the feasibility of a high-gain facility.

The LLE OMEGA laser is the only major facility in the United States capable of currently conducting fully diagnosed, symmetric, direct-drive, spherical implosion experiments. The 1986 National Academy of Sciences (NAS) Report of the Committee for a Review of the Department of Energy's Inertial Confinement Fusion Program concluded that if the LLE program achieved the challenging goal of attaining 100–200 times liquid DT density in compression experiments, they would support a 30,000-J upgrade of OMEGA for the purpose of demonstrating significant thermonuclear burn via direct drive. Calculations indicate that a 30,000-J, ultraviolet (UV) laser system could produce implosions in the ignition regime (see Fig. 38.1). In addition, such a facility could support a number of multi-laboratory collaborative experiments to investigate many important ICF issues, such as ignition scaling, fuel-pusher interface mix, preheat, and hydrodynamic instabilities.

In 1988, the objective of 100–200 times liquid DT density was attained on the OMEGA laser with cryogenic fuel targets; high compression was verified using a number of independent measurement



E4484

Fig. 38.1

The quality of fuel confinement for inertial fusion is the fuel areal density—the product of fuel density  $\rho$  (in grams per cubic centimeter) times the compressed fuel radius  $R$  (in centimeters). Thermonuclear microcore ignition requires a fuel- $\rho R$  product in excess of  $0.3 \text{ g/cm}^2$  at temperatures higher than  $5,000 \text{ eV}$ . The progress of direct-drive ablative compression on the OMEGA laser in achieving the required degree of fuel compression ( $\rho R$ ) is shown. OMEGA experiments at  $1,000 \text{ J}$ – $1,500 \text{ J}$  with cryogenic-fuel-layer targets have demonstrated a fuel  $\rho R$  of  $0.03 \text{ g/cm}^2$ . Near-ignition conditions could be achieved by the upgraded OMEGA laser operating at a level of  $30,000 \text{ J}$ .

techniques. These experiments were the result of an intensive effort, which included (a) improvements of the target surface distribution of laser irradiation on the OMEGA laser; (b) the development and implementation of a new class of diagnostic instrumentation to measure high-density implosions; and (c) the implementation of cryogenic fuel-layer technology on the OMEGA facility. The results of these experiments were validated by a DOE-selected panel of scientists from other ICF laboratories.

The proposed upgrade of the OMEGA facility is based on the Nd:glass laser technology developed over the last decade by LLNL and LLE. Preliminary design engineering and development and studies of the upgrade to OMEGA began in FY88; full implementation of the facility could occur by 1992. The cost estimates initially proposed (final estimates to be defined by the design study) are  $\$39,000,000$  (in

FY88 dollars) [or a total of \$44,120,000 in as-spent dollars]. A key objective of the upgrade engineering design is to keep the added operating costs of the facility as low as possible.

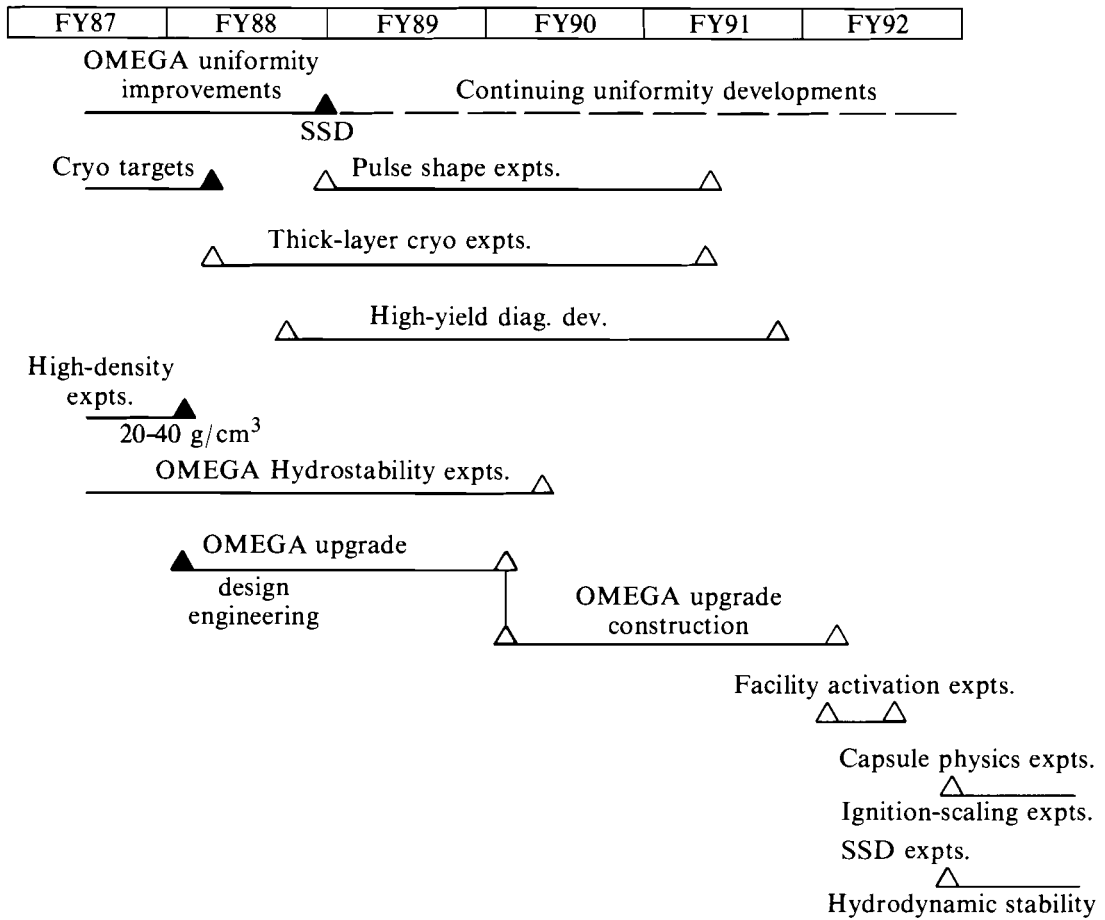
### **Program Plan for the OMEGA Upgrade**

Direct drive for laser fusion provides a singular opportunity to define the minimum energy required to build a successful ICF facility. As the principal focus of the DOE research on direct drive, the whole research effort at LLE is designed to address the important questions of driver and target performance needed to produce high-density implosions. The four elements of the LLE direct-drive ICF program are

1. OMEGA Upgrade engineering and development,
2. OMEGA experiments and laser operations,
3. target fabrication, including cryogenic fuel-layer capsule development, and
4. high-density target diagnostic development and implementation.

Modifications to the OMEGA facility include implementation of pulse-shaping systems; multibeam pulse-shape diagnostics; beam-uniformity improvements; and the design, development, fabrication, and activation of a 30,000-J upgrade to the OMEGA laser. The engineering design effort for this element will be completed this year. Full implementation of the OMEGA upgrade could begin in FY90 with completion by FY92, according to the schedule illustrated in Fig. 38.2.

In planning the OMEGA upgrade, LLE will continue to emphasize Nd:glass laser technology. Primary emphasis will be on designing and testing high-efficiency amplifier modules for potential use in the upgrade. LLE will be collaborating with LLNL on this effort; in one aspect of this collaboration, LLE will evaluate a version of a LLNL-proposed disk amplifier for use on the upgraded laser. The development of measurement and design techniques for improving the quality of glass drivers will be continued. The LLE engineering division will investigate new and improved methods of producing optical components, such as mirrors, polarizing elements, mechanical supports, phase plates, and other systems needed to operate large fusion-laser systems. In addition to creating an enhanced experimental capability, the upgrade of the OMEGA laser will provide the opportunity to augment the ICF driver-development effort and to test many advanced glass-laser concepts relevant to a laboratory high-gain facility.



E4330

Fig. 38.2  
 Schedule for the LLE direct-drive laser-fusion program including the upgrade of the OMEGA laser system.

## 1.A Direct-Drive, High-Gain, Hydrodynamics Equivalent Experiments Facility

Over the past several years the inertial confinement fusion (ICF) program has made significant progress in addressing a number of key physics issues. These advances have made it possible for the Department of Energy (DOE) to begin to address the requirements needed to achieve ICF's major objective—high gain in the laboratory. To date, a large effort has been devoted to the understanding, both experimentally and theoretically, of the national program's main approach to ICF—indirect drive.<sup>1</sup> However, recent achievements in directly driven capsule implosions<sup>2,3</sup> and the development and initial implementation of laser-beam-smoothing techniques<sup>4-7</sup> have shown that a direct-drive solution to the national program's goal, along with its potential savings in driver energy, deserves increased attention.

At present there are a number of key physics issues associated with high-gain, direct-drive pellet implosions for which little, if any, experimental data exists. This information is required by DOE to better determine the future role of direct drive. Here we present these physics issues as they pertain to a direct-drive, high-gain pellet implosion and discuss why a new direct-drive experimental facility is required to obtain this data base. Subsequent articles in this and the next LLE Review will present how this facility could be constructed as an upgrade to the present OMEGA laser facility, as well as preliminary design concepts of the implementation of many system features.

This article is divided into two sections: First, using a numerical simulation of a high-gain, direct-drive pellet implosion, the key physics issues, requiring increased experimental data, are presented. Second, the general requirements that a direct-drive facility will have to meet to carry out the relevant experiments are examined.

### One-Dimensional, High-Gain, Direct-Drive Designs

Recently, several high-gain, direct-drive pellet designs, spanning an incident-energy range of 1.0 to 10.0 MJ, have been examined for both 351-nm and 270-nm illumination. They are all single-shell designs consisting of a low-atomic-number ( $Z$ ) ablator surrounding a levitated cryogenic deuterium-tritium (DT) main fuel layer. The inner region of the pellet contains a DT-gas mixture whose density and composition are determined by the temperature of the main fuel layer. (Several designs were carried out with the main fuel composed of a DT/low-density CH foam mixture.<sup>8</sup> For this article, we limit discussion to pellet designs for which the main fuel layer is pure DT.)

The designs were carried out using the one-dimensional hydrodynamic code *LILAC*. *LILAC* contains Lagrangian hydrodynamics, tabular equation of state (SESAME),<sup>9</sup> thermonuclear

burn, multigroup particle transport, and multifrequency radiation transport. The opacities used in the multifrequency transport are obtained from reducing the Los Alamos National Laboratory (LANL), 2000-frequency-group, local thermodynamic equilibrium (LTE), Astrophysical Library<sup>10</sup> to a desired group structure ( $\sim 50$  groups are used for the simulations presented in this article). Laser-energy deposition is modeled by a geometric optics ray-trace algorithm<sup>11</sup> with energy deposited by inverse Bremsstrahlung along the ray path. Flux limitation of electron thermal transport<sup>12</sup> is incorporated as a “sharp cutoff” with the Spitzer-Härm electron thermal conductivity. [For the simulations presented in this article the value of the flux limiter  $f$  is set to 0.06 with the maximum permitted heat flux given by  $q_{\max} = f n_e kT(kT/m_e)^{1/2}$ . This value of  $f$  has been found to give the best numerical results of laser-energy absorption, x-ray conversion for moderate-Z materials, and hydrodynamic motion of recent OMEGA pellet implosions.<sup>3,13</sup>]

The first issue is to determine the effect of irradiation nonuniformity on direct-drive target implosions. Two-dimensional simulations of direct-drive pellet implosions show that illumination nonuniformities can adversely affect pellet implosion by two principal means. The first is development of long-wavelength ( $\ell \leq 8$ ), secular ( $t^2$ ) growth during the acceleration phase caused by variations in the drive pressure. The second is the seeding of short-wavelength modes that can then develop due to the Rayleigh-Taylor<sup>14-16</sup> instability at the ablation surface. Current two-dimensional simulations of high-gain, direct-drive pellet implosions indicate that illumination nonuniformities on target will have to be  $\leq 1\% \sigma_{\text{rms}}$ .<sup>17</sup>

Several investigators have examined the uniformity produced by overlapping multiple laser beams on spherical targets.<sup>18-22</sup> Research at LLE has emphasized the decomposition of the laser energy in terms of spherical harmonics to obtain information about the spatial wavelengths of the nonuniformity on target for a beam-overlap pattern.<sup>22</sup> The irradiation pattern on target can be expressed as the product of two factors: (1) a “single-beam” factor that depends on the focal position,  $f$ -number of the lens, assumed target conditions, energy and possible temporal imbalance between individual beams (power balance), and the individual beam profiles; and (2) a “geometric” factor that is determined by the number and orientation of the individual beams about the target.

Analysis of different beam configurations for given focus conditions and laser-beam profiles, has shown that increased uniformity can be obtained over a wider focal region by increasing the number of beams. Figure 38.3 shows the predicted rms illumination nonuniformity on target for 20, 32, 60, and 96 beams using an ideal quadratic radial-beam profile. All beam configurations provide adequate uniformity at a focus ratio of  $\sim 1$  (tangential focus). However, during capsule implosion, the focus ratio shifts (toward the right along the abscissa in Fig. 38.3) because of the inward motion of the critical surface. Due to this motion, a system with significantly less than 60 beams, unlike the 60- and 96-beam configurations, fails to provide the required drive

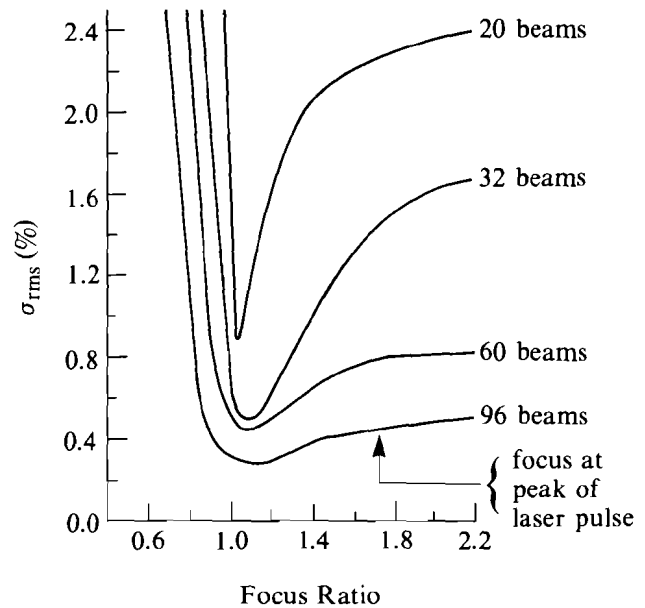


Fig. 38.3  
Illumination uniformity as a function of focus position for 20-, 32-, 60-, and 96-beam geometries having 2% solid angle fraction.

A97

uniformity throughout the pellet implosion. These simulations do not include the possible effects of thermal smoothing<sup>23</sup> of illumination nonuniformities in the pellet corona. While further experimental and theoretical understanding of the role of thermal smoothing would possibly allow for the use of less than 60 beams, when factors such as power imbalance and individual beam mispointing are included in the uniformity calculations, systems with substantially less than 60 beams fail to provide the necessary illumination uniformity over the duration of the implosion.

Since our laser system has a fixed number of beams, much of our research effort has been devoted to understanding, modifying, and controlling the single-beam factor.<sup>4-7</sup> Controlling power balance and the individual laser-beam profiles has shown great promise for future direct-drive implosions. Implementation of both a more stringent control of power balance and an initial form of beam smoothing [smoothing by spectral dispersion (SSD)<sup>7</sup>] has resulted in improved target performance for gas-fuel, glass-pusher experiments on OMEGA.

Understanding both the effects of illumination nonuniformity on pellet performance and how to reduce and control the level of illumination nonuniformity on target represents an extremely important physics issue for which more information is required. Our discussion of uniformity has been presented independent of a particular high-gain design. Simulations have shown that the required level of illumination uniformity is approximately the same for all high-gain designs in the energy range of 1.0 to 10.0 MJ.

Theoretical and experimental work is under way at LLE to continue to improve the single-beam factor associated with illumination uniformity on OMEGA. Based on our understanding of how to control power balance and improve individual beam profiles, the current OMEGA laser system does not provide adequate illumination uniformity to perform experiments that are hydrodynamically similar to that of a high-gain pellet.

Three key physics issues can best be presented by using a particular high-gain, direct-drive pellet design. As an example, we examine the single-shell, CH-ablator design shown schematically in Fig. 38.4(a). The applied laser pulse, shown in Fig. 38.4(b), is temporally shaped over  $\sim 45$  ns and contains  $\sim 3.4$  MJ of ultraviolet (351-nm) light. This pulse, shown in Fig. 38.4(b), has been optimized to maximize the overdense shell thickness, while maintaining a low-fuel isotrope, with minimum laser intensity on target. The calculated absorption efficiency ( $\eta_a$ ) for this implosion is  $\sim 90\%$ . The laser intensities at the quarter- and tenth-critical surfaces are shown in Fig. 38.4(c). These intensities represent the total intensity on target while the peak intensities for each individual beam would be  $\sim 4 \times 10^{13}$  W/cm<sup>2</sup>, well below the threshold for plasma instabilities.

Laser-light coupling and possible detrimental plasma physics effects during a direct-drive, high-gain implosion represent a second key physics issue for which little experimental data exists. Experimental and theoretical comparisons show that observables, such as the absorption efficiency, can be adequately modeled using inverse Bremsstrahlung and a ray-trace treatment. Current direct-drive implosion experiments are carried out on implosions that have extremely short-density scale lengths in comparison with high-gain designs. While a large number of theoretical simulations and calculations have been performed to estimate the effects of laser light transversing large-density scale lengths, little or no experimental data exists for density scale lengths/intensity regimes found in MJ-scale, high-gain capsule implosions. What experiments have been carried out on long-scale-length plasmas were done with laser-beam profiles that would not be adequate for high-gain, direct-drive. Extrapolating from these experiments could prove faulty because some of the observables may have been influenced by the poor quality of the laser beams used in the experiments.

The next key physics issue considered is hydrodynamic stability and its effect on high-gain pellet implosions. Figure 38.4(d) displays the in-flight aspect ratio as a function of time for the 3-MJ implosion. The in-flight aspect ratio can be considered to represent a measure of the target's ability to withstand shell breakup due to the Rayleigh-Taylor hydrodynamic instability. The in-flight aspect ratio is defined as  $A(t) = R(t)/\Delta R(t)$ , where  $\Delta R(t)$  is found by first determining the radial location and value of the peak material density in the imploding pellet. The positions for density values of  $1/e$  of the peak determine  $\Delta R(t)$ , and the average of these two locations is  $R(t)$ . This definition accounts for  $\sim 77\%$  of the imploding shell mass, the cold fuel layer, and the pusher surrounding the central hot-spot region. Rayleigh-Taylor

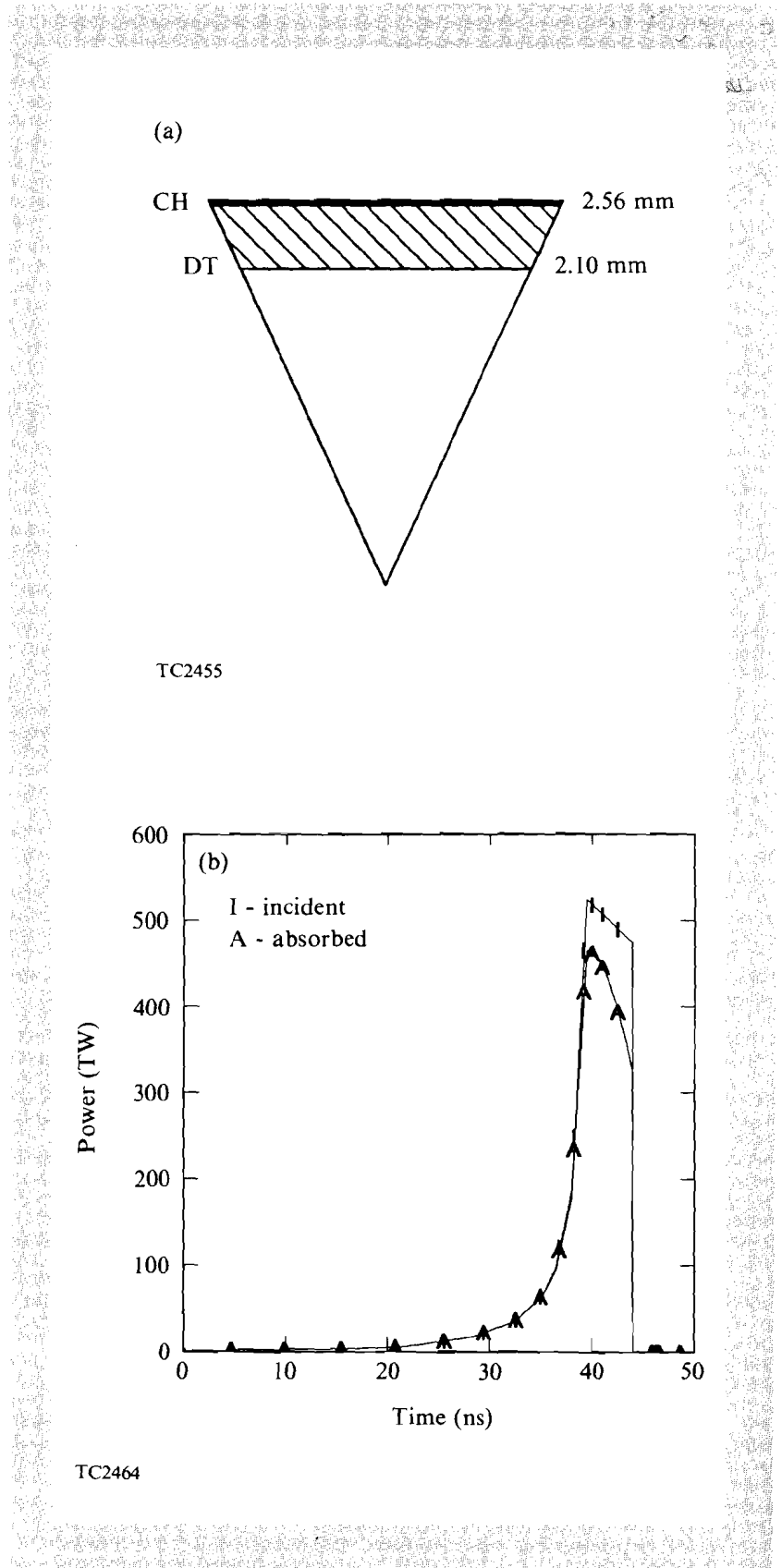
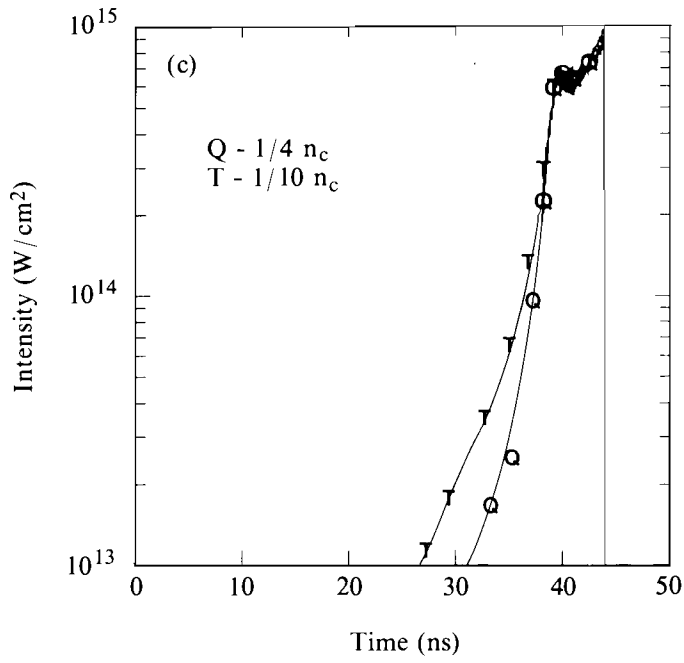
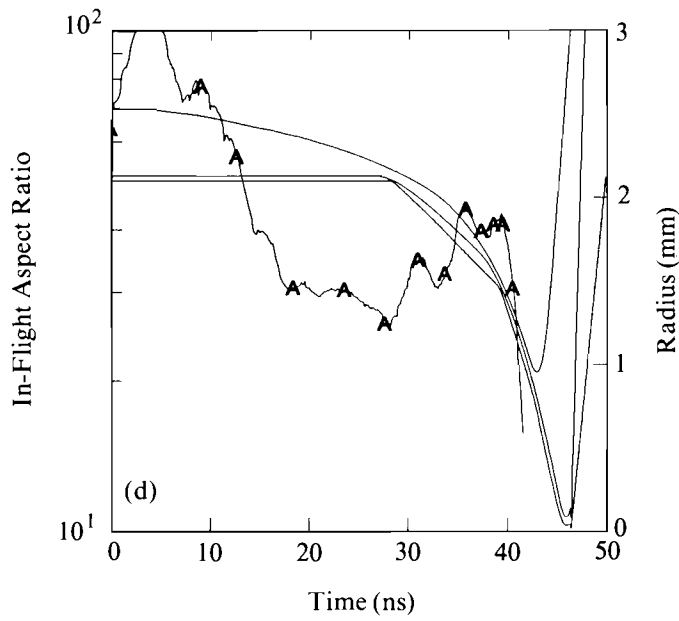


Fig. 38.4  
 One-dimensional (*LILAC*) hydrodynamics simulation of a 3-MJ, 351-nm, single-shell, direct-drive, high-gain design.  
 (a) Schematic of pellet.  
 (b) Temporal pulse shape: *I*-incident, *A*-absorbed.  
 (c) Laser intensity at  $\frac{1}{4}$  critical density (*Q*) and  $\frac{1}{10}$  critical density (*T*).  
 (d) In-flight aspect ratio and layer-radii in-flight aspect ratio (*A*).



TC2459

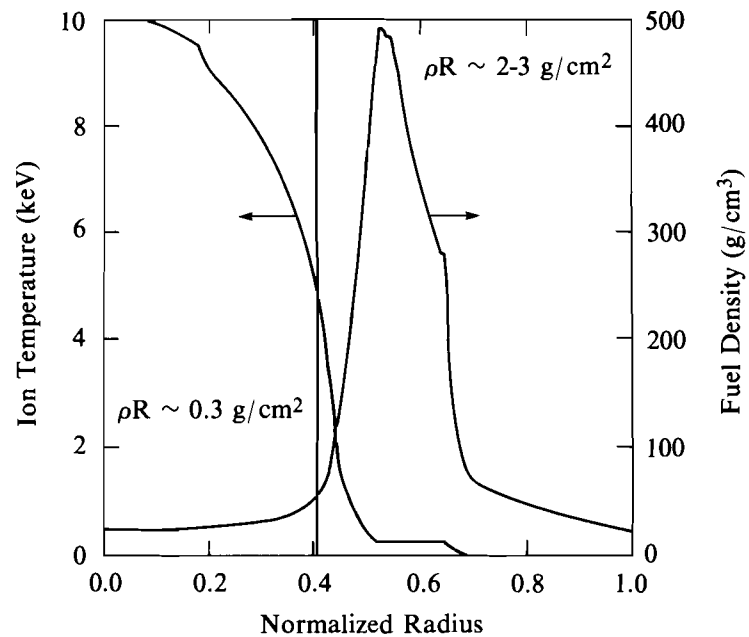


TC2476

unstable growth of this material into the main fuel mass during the acceleration and deceleration phases is important to determine pellet performance. [The algorithm used to determine  $A(t)$  will pick up and follow shocks that are moving through the overdense fuel pellet during the acceleration phase. This results in what appears to be large values of the in-flight aspect ratio for short periods of time and can be seen in Fig. 38.4(d) as the spike-like structures at  $t < 10$  ns when the “first” shock is moving through the pellet and again at 30, 35, and 40 ns.] The in-flight aspect ratio for this design peaks at  $\sim 40$  during the time of maximum acceleration. A large number of theoretical calculations of the development and effects of the Rayleigh-Taylor instability on direct-drive pellet implosions<sup>24-26</sup> have, in general, found that the growth of the instability, in the presence of ablation, is reduced when compared to the classical value. Simulations have shown that the effects of the instability will, in general, depend on the growth and possible mode-mode interactions of all of the modes that are seeded (both by illumination nonuniformities and target imperfections) during the implosion.

Whether the present target design with a peak in-flight aspect ratio of 40 will survive the effect of Rayleigh-Taylor unstable growth during the acceleration phase will depend on the spectrum, initial amplitudes, and amplification of the seeded modes. At this time, these important factors can only be estimated theoretically. A limited number of important Rayleigh-Taylor experiments<sup>27-29</sup> have been carried out on direct-drive targets. However, due to the complexity of both the experiments and their interpretation, these represent a very limited set of data against which direct-drive simulations can be compared.

A final key issue for which no laboratory data currently exists is the physics associated with hot-spot formation and ignition of a direct-drive, high-gain design. At the culmination of the implosion, the imploding fuel material (all of the CH ablator has been ablated away by this time) is typically moving inward with a mass-averaged velocity of  $\sim 3.0 \times 10^7$  cm/s. The shock energy, kinetic energy, and pressure-volume work associated with the imploding shell, balanced against radiative and conductive losses, are transformed into internal energy of the hot-spot material. For these designs the hot spot is composed of the initially gaseous material and a thin layer of material that was initially located at the very inner edge of the main fuel layer. Figure 38.5 schematically displays the conditions of the hot spot and main fuel layer at the time of ignition. In the hot spot, the ion temperature is usually between 5 keV and 10 keV with a density of  $\sim 60$  g/cm<sup>3</sup>. At these temperatures, densities, and fuel areal densities ( $\rho R$ ), the alpha particles from thermonuclear reactions begin to redeposit their energy in the hot spot. As this happens, the hot spot begins to self-heat, resulting in further fusion reactions, which deposit their energy in a region just outside of the hot spot, which results in the rapid heating of the surrounding fuel (“boot strapping”). Newly created alpha particles deposit their energy further out in the fuel while fuel layers adjacent to the hot spot begin to burn, producing more alpha particles and more heat. Thus, a thermonuclear burn wave propagates outward consuming the remaining fuel material. The fuel eventually disassembles as a



TC2563

Fig. 38.5

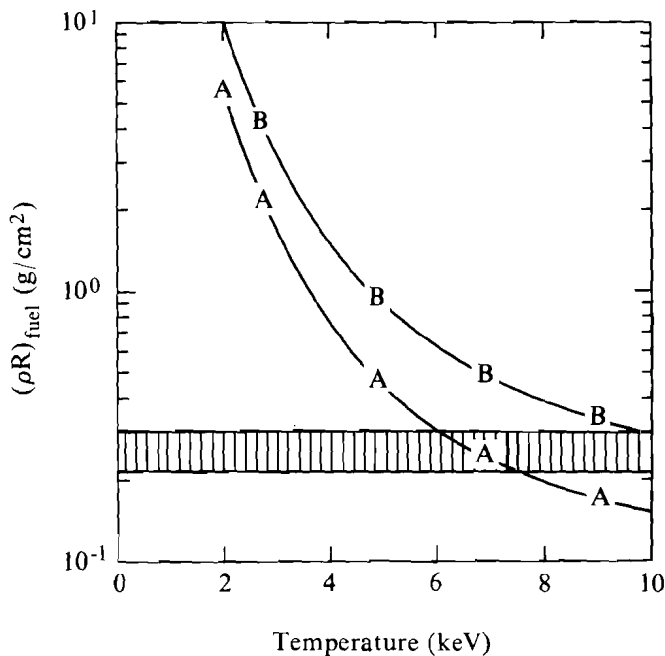
Schematic of hot-spot region near time of ignition for high-gain pellet design composed of DT.

rarefaction wave propagates back through the fuel to the origin. Two-dimensional numerical simulations of these pellet designs (composed of only DT during the final stagnation phase) show that, if the spark plug ignites, the radially outward-propagating burn wave will result in essentially “1-D” yields even if the main fuel layer is moderately distorted.

Simulations have shown that the hot spot will fail to ignite if large perturbations are present during the formation of the spark plug.<sup>17</sup> The presence of long-wavelength perturbations ( $\ell < 8$ ) can cause the internal energy of the fuel forming the hot spot to be converted into kinetic energy due to incoming, distorted, “cold” DT from the main fuel layer. Calculations indicate that the mixing of cold and hot DT, due to the Rayleigh-Taylor instability during the deceleration phase of implosion, can preclude ignition. Experimental data are required to increase understanding of important processes in hot-spot formation and ignition. This issue is tied to all of the three key physics issues we have discussed. Illumination nonuniformity can cause secular or Rayleigh-Taylor unstable growth, which can adversely affect pellet performance during the acceleration phase and subsequently the hot-spot formation during the deceleration phase. Any error in our understanding of the absorption of the laser light and, eventually, the energy available to the fuel will have important effects on the required

energy to drive a given high-gain pellet. The high-gain design presented in this section was carried out using our current "best" theoretical understanding of these key physics issues. It is clear, however, that until our understanding is confirmed by experiments, there will always be some question about the validity of such designs.

In order to obtain the experimental data base and theoretical understanding of the four key physics issues, any new direct-drive experimental facility will, in addition to carrying out well-diagnosed pellet implosions, have to be both a laser illumination uniformity and pulse-shaping "test bed." To estimate the amount of drive energy required by this system, if all four of the key physics issues presented previously are to be addressed, we first examine the issue of hot-spot physics/ignition scaling. The hot spot of a direct-drive, high-gain design is both hot (5 keV to 10 keV) and dense (~300 times liquid density). These conditions place constraints on the minimum energy of the system. Using the definition of ignition put forth by Nuckolls<sup>30</sup> [ignition is defined to occur when the liberated alpha-particle energy redeposited back into the fuel equals the energy invested to compress the fuel ( $E_{\text{fuel}} \approx 1/5 E_{\text{fusion}}$ )], one can obtain an estimate of the required fuel temperature and areal density. This is shown in Fig. 38.6 where the hatched region represents the fuel  $\rho R$  region between ~0.2 and 0.3 g/cm<sup>2</sup>. The driver energy can then be estimated as a function of coupling efficiency ( $\eta_c = \eta_a \eta_H$ , where  $\eta_H$  is the hydrodynamic



TC2407

Fig. 38.6  
 Fuel areal density ( $\rho R$ ), temperature regime of ignition based on the definition in Ref. 30. A: confinement time given as  $R/C_s$ ; B: confinement time given as  $R/(2C_s)$ .

efficiency) and compression for a given temperature, fuel  $\rho R$ , and disassembly time multiplier [ $E_{\text{driven}} \propto 1/\eta_c(\rho_{\text{fuel}})^2$ ]. As an example, the driver energy required for a fuel temperature of 7 keV and a disassembly time given by  $R/C_s$  (where  $R$  is the fuel radius and  $C_s$  is the sound speed) is shown in Fig. 38.7. For coupling efficiencies between that predicted for the 351-nm, high-gain, direct-drive designs presented in Sec. 1 and modest compressions, laser energies between 20 kJ and 100 kJ are required to meet the Nuckolls definition of ignition. (One could reduce the laser energy by increasing the compression; however, hydrodynamic-stability issues could place severe constraints on achieving such high compressions.) These simple estimates indicate that, in order to examine physics issues related to hot-spot formation and ignition, laser energies in excess of 20 kJ on target will be required.

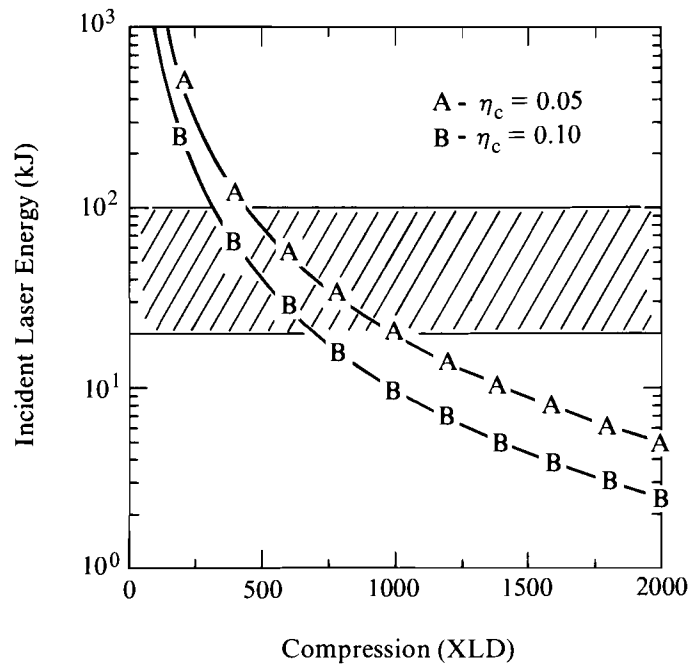


Fig. 38.7

Incident laser energy versus compression for ignition at a temperature of 5 keV and confinement time given by  $R/C_s$ . A: coupling efficiency ( $\eta_c$ ) = 0.05; B: coupling efficiency = 0.10.

TC2427

Having identified an energy threshold for this facility, one can then investigate hydrodynamically equivalent pellet designs, that is designs whose physical behavior scales to those appropriate for high gain. If a target is described by its hydrodynamic behavior alone, it can be scaled in size by the following relations:

$$\begin{aligned} \text{Energy: } E &\propto R^3 \\ \text{Power: } P &\propto R^2 \\ \text{Time: } t &\propto R \end{aligned}$$

This scaling, while not strictly valid because of changes associated with transport processes during implosion and thermonuclear reaction and transport processes during the burn phase, serves as a starting point for a 30-kJ, high-gain, hydrodynamic-equivalent design obtained by scaling the 3-MJ design presented in the previous section. The two pellets are shown in Fig. 38.8 (note sizes are not to scale). Similarly, the pulse shape shown in Fig. 38.4(b) was scaled down resulting in the curve labeled *S* in Fig. 38.9. One- and two-dimensional simulations show that this energy-scaled pellet design has a similar in-flight aspect ratio  $\leq 40$ , a hot-spot convergence ratio  $\leq 25$ , and the same uniformity requirements as the 3-MJ design. The solid, unlabeled curve in Fig. 38.9 represents a pulse consisting of two Gaussian pulses truncated at  $\sim 6.5$  ns. This pulse shape, while not possessing all of the desired characteristics of the scaled pulse, has been shown numerically to be a good “initial” approximation to the pulse shape that the new facility should have.

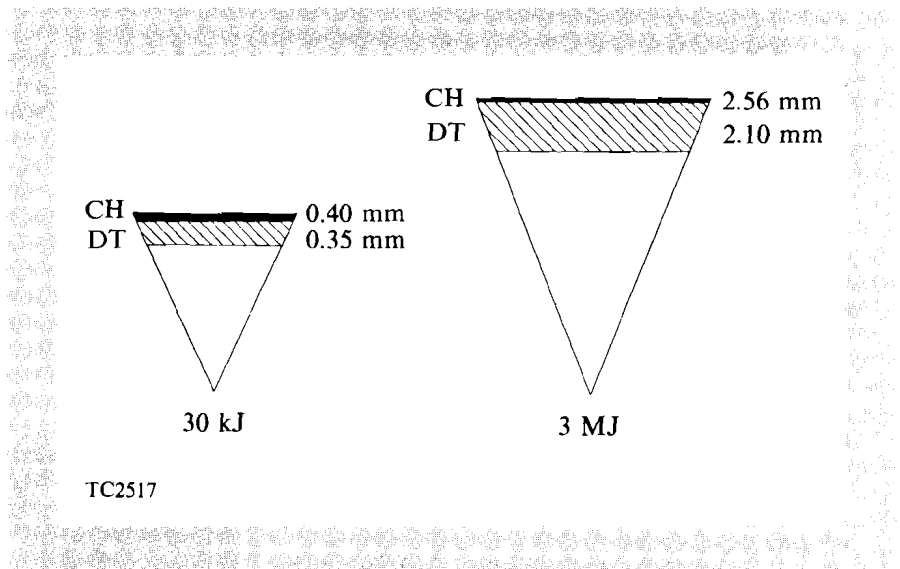


Fig. 38.8

Schematic of energy-scaled, 30-kJ, hydrodynamic-equivalent pellet design and initial 3-MJ pellet design. Note pellets are not drawn to scale.

Current theoretical work associated with SSD has shown that, with further modifications and the use of 60 beams, illumination nonuniformities could be reduced to the level required to do relevant hydrodynamic-equivalent experiments ( $\sim 1\%$  to  $2\%$   $\sigma_{rms}$ ). The facility should be designed with enough flexibility to allow for changes to be made to the single-beam factor (principally the individual beam profiles) so that illumination-uniformity improvements could be incorporated as they become available.

The energy-coupling issues presented in the first section would have to be addressed in two parts. The energy-scaled target presented in Fig. 38.8 would not have a scale length as large as that of the high-gain design. However, the experimental data associated with energy coupling obtained on the hydrodynamic-equivalent targets (which have

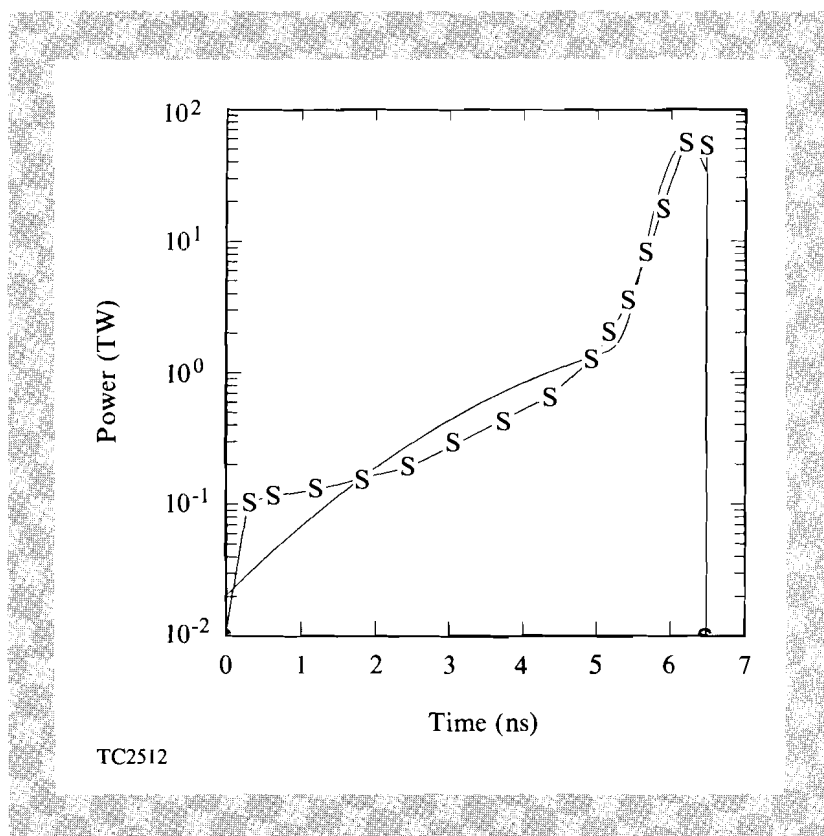


Fig. 38.9

Energy-scaled pulse shapes. *S* represents the scaled 3-MJ pulse shape; the solid curve represents a pulse shape constructed of two truncated Gaussian pulses, which could serve as the initial pulse shape the system could produce.

density scale lengths larger than those of present direct-drive experiments) would serve as an additional check of our understanding of how laser light couples to the target. Issues more relevant to the density scale length/intensity regime associated with high-gain designs could also be addressed using flat targets and a limited number of laser beams, similar to techniques successfully used on NOVA.<sup>31</sup> Such experiments could generate long-scale-length plasmas using individual laser beams more characteristic of those of high-gain, direct-drive implosions.

We believe that a 30-kJ, 351-nm, 60-beam laser system can provide the necessary experimental data base required to determine the role of direct-drive in future ICF planning. While the issues presented in this article were limited to direct drive, it is evident that the data base obtained from such a facility would also prove important in understanding processes associated with high-gain, indirect-drive pellet implosions. Subsequent articles in this and the next LLE Review will discuss in more detail the design of the OMEGA upgrade.

#### ACKNOWLEDGMENT

This work was supported by the U.S. Department of Energy Office of Inertial Fusion under agreement No. DE-FC03-85DP40200 and by the Laser Fusion Feasibility Project at the Laboratory for Laser Energetics, which has the following sponsors: Empire State Electric Energy Research Corporation, New York State Energy Research and Development Authority, Ontario Hydro, and the University of Rochester. Such support does not imply endorsement of the content by any of the above parties.

## REFERENCES

1. J. H. Nuckolls, *Phys. Today* **35**, 24 (1982).
2. R. L. McCrory, J. M. Soures, C. P. Verdon, F. J. Marshall, S. A. Letzring, S. Skupsky, T. J. Kessler, R. L. Kremens, J. P. Knauer, H. Kim, J. Delettrez, R. L. Keck, and D. K. Bradley, *Nature* **335**, 225 (1988).
3. LLE Review **35**, 97 (1988).
4. R. H. Lehmborg and S. P. Obenschain, *Opt. Commun.* **46**, 27 (1983).
5. Y. Kato *et al.*, *Phys. Rev. Lett.* **53**, 1057 (1984).
6. LLE Review **33**, 1 (1987).
7. LLE Review **37**, 29 (1989).
8. R. A. Sacks and D. H. Darling, *Nucl. Fusion* **27**, 447 (1987).
9. B. I. Bennett, J. D. Johnson, G. I. Kerley, and G. T. Rood, Los Alamos National Laboratory Report LA-7130 (1978).
10. W. F. Huebner, A. L. Merts, N. H. Magee, and M. F. Argo, Los Alamos National Laboratory Report LA-6760-M (1977).
11. M. Born and E. Wolf, *Principles of Optics* (Pergamon, New York, 1975), p. 123.
12. R. C. Malone, R. L. McCrory, and R. L. Morse, *Phys. Rev. Lett.* **34**, 721 (1975).
13. C. P. Verdon, F. J. Marshall, S. Letzring, D. K. Bradley, J. Delettrez, R. L. Keck, J. P. Knauer, R. L. Kremens, R. L. McCrory, S. Skupsky, and J. M. Soures, *Bull. Am. Phys. Soc.* **33**, 2006 (1988).
14. G. J. Taylor, *Proc. R. Soc. London, Ser. A* **201**, 192 (1950).
15. D. J. Lewis, *Proc. R. Soc. London, Ser. A* **202**, 81 (1950).
16. S. Chandrasekhar, *Hydrodynamic and Hydromagnetic Stability* (Clarendon Press, Oxford, England, 1961), Chap. 10.
17. LLE Review **23**, 125 (1985).
18. Lawrence Livermore Laboratory Laser Program Annual Report UCRL-50021-74, p. 219 (1975).
19. J. Howard, *Appl. Opt.* **16**, 2764 (1977).
20. A. J. Scannapieco and H. Brysk, *J. Appl. Phys.* **50**, 5142 (1979).
21. K. Lee, R. L. McCrory, and R. Hopkins, Laboratory for Laser Energetics Report No. 88 (1981).
22. S. Skupsky and K. Lee, *J. Appl. Phys.* **54**, 3662 (1983).
23. S. E. Bodner, *J. Fusion Energy* **1**, 221 (1981).
24. M. H. Emery, J. H. Gardner, and J. P. Boris, *Phys. Rev. Lett.* **48**, 677 (1982).

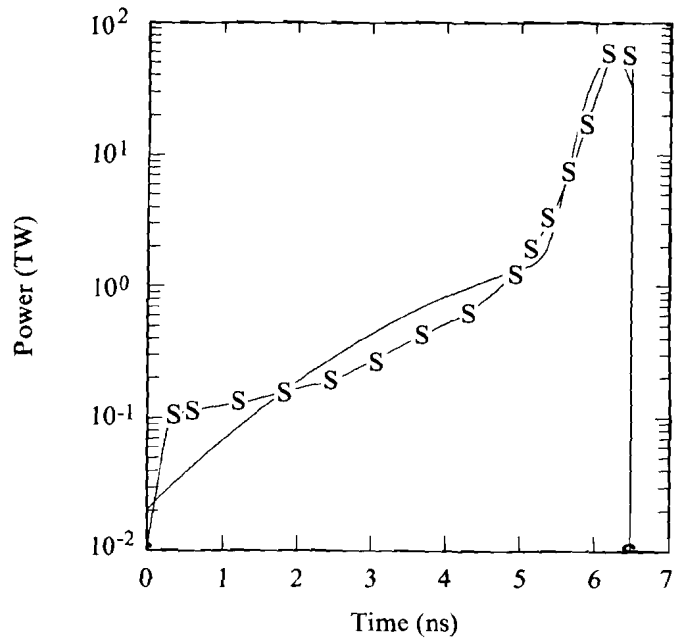
25. C. P. Verdon, R. L. McCrory, R. L. Morse, G. R. Baker, D. I. Meiron, and S. A. Orszag, *Phys. Fluids* **25**, 1653 (1982).
26. H. Takabe, K. Mima, L. Montierth, and R. L. Morse, *Phys. Fluids* **28**, 3676 (1985).
27. A. J. Cole *et al.*, *Nature* **299**, 329 (1982).
28. R. R. Whitlock *et al.*, *Phys. Rev. Lett.* **52**, 819 (1984).
29. J. Grun *et al.*, *Phys. Rev. Lett.* **53**, 1352 (1984).
30. J. H. Nuckolls, Lawrence Livermore National Laboratory Report, UCRL-84932 (1980).
31. R. P. Drake *et al.*, *Phys. Fluids* **31**, 1795 (1988).

## 1.B Laser Design and Performance

As discussed in article 1.A, important ignition physics issues could be investigated with a laser system capable of uniformly targeting 30 kJ of ultraviolet (UV, 351-nm) light with the temporal pulse shape illustrated in Fig. 38.10. The design of such a laser system presents several challenges. The first challenge is to generate the required energy at the lowest possible cost. As discussed below, while the implosion experiment utilizes 30 kJ of UV energy on target, the overall laser output, because of inherent system losses and red-to-blue conversion efficiencies, must be in excess of 60 kJ in the infrared (IR, 1054 nm). Production of such energies will be facilitated by the design, testing, and implementation of the multisegmented amplifier (MSA). This new amplifier,<sup>1</sup> a joint effort between Lawrence Livermore National Laboratory (LLNL) and the University of Rochester Laboratory for Laser Energetics (LLE), will be discussed in detail below.

The next important challenge is the generation of the desired on-target temporal pulse shape. The target design group has determined a set of basic requirements for the general pulse shape. The on-target pulse shape will be synthesized from two independent sub-pulses. Special attention must be given to minimize the damage threat associated with each of the sub-pulses. Such considerations will determine the location and size of certain optical components in the chain as well as many of the materials used.

The final challenge is to meet the stringent uniformity requirements of the implosion dynamics. It has been shown that the overall illumination uniformity of a laser system improves significantly as the number of incident beams is increased.<sup>2</sup> To take advantage of this, it



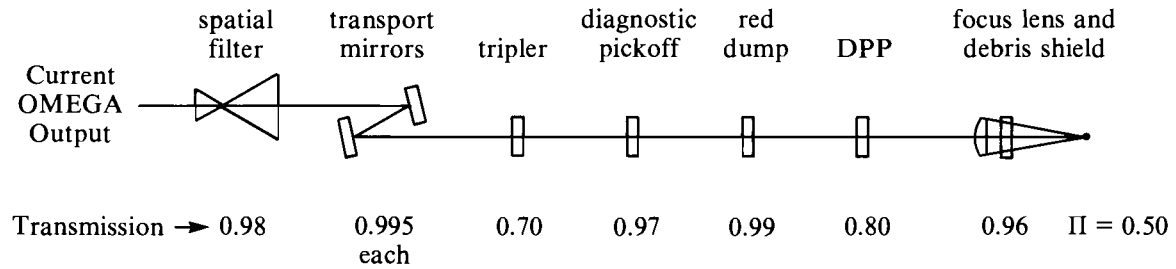
TC2512

Fig. 38.10  
Required on-target temporal pulse shape(s)  
scaled from MJ pulse shape and double-  
Gaussian approximation to it.

is planned to increase the number of beams on the OMEGA system (currently 24 beams). By comparing the increasing cost associated with handling larger number of beams with the improving uniformity, it was determined that the OMEGA upgrade would place 60 beams on target. This decision is complicated by two additional issues. First is the issue of producing both sub-pulses in each of the 60 beams. Second is the requirement that maximum use be made of the existing OMEGA hardware and laser-bay floor space. The easy solution of building two independent, 60-beam laser systems and combining them on target was rejected because of prohibitive costs and insufficient laser-bay area. The solution we have adopted is the co-propagation of two pulses in physically separate regions of the same beamline. This concept is the most cost-effective method (one laser system that can occupy the existing laser bay) of achieving the given uniformity requirements while still providing for all other parameters essential to the upgrade.

### Laser Output Requirements

Although the designed, on-target energy is 30 kJ, the losses associated with the laser components between the target and the final amplifier must be accounted for in determining the final amplifier output energy. An output-energy budget for the proposed system is shown in Fig. 38.11. The output of the amplifier must be transported, frequency converted, diagnosed, focused, and phase converted. Nonlinear effects in air and the paucity of high-damage-fluence, 351-nm, high-reflector coatings dictate that frequency conversion take



- 50% of final amplifier output reaches target.

G2484

Fig. 38.11  
Output energy budget.

place at or near the target chamber. The collective transport losses of the final spatial filter, transport mirrors, diagnostic, and focusing lens at 1054 nm are typically 10%. The target is placed in the central focal spot of a distributed phase plate (DPP), a phase mask located after the focusing lens, which contains 80% of the energy incident on the DPP. The frequency-conversion process can achieve a theoretical maximum of 80% efficiency for these temporal shaped pulses. Since a number of effects can degrade tripling efficiency,<sup>3,4</sup> a conservative 70% tripling efficiency has been assumed. The product of these effective transmissions is 50%, i.e., the energy output of the final amplifier must be twice the target requirement. If the foot and main pulses are delivered by separate beamlines, the energy per beam for the main pulse is 800 J and 200 J for the foot pulse, or 1000 J for a combined beamline.

### MSA Amplifier

The MSA proposed for the OMEGA Upgrade is shown in Fig. 38.12. Because of the very close packing of adjacent beams in the MSA architecture, magnification and injection into the next amplifier stage requires either special handling optics after the amplifier to separate the beams or a very large, clear-aperture spatial filter. This problem can be avoided by using the MSA in an angularly double-passed configuration. This configuration allows amplification of the output of a current OMEGA beamline to the required levels in one stage. The angular offset may be taken on the output beam to provide the necessary beam separation for subsequent magnification. An increase in the amplifier clear aperture is necessary in order to accommodate the beam offset. If the required beam separation at the end of the stage is set equal to the amplifier's (not the beam's) clear aperture, then a relation may be derived between the required propagation distance for beam separation and amplifier clear aperture

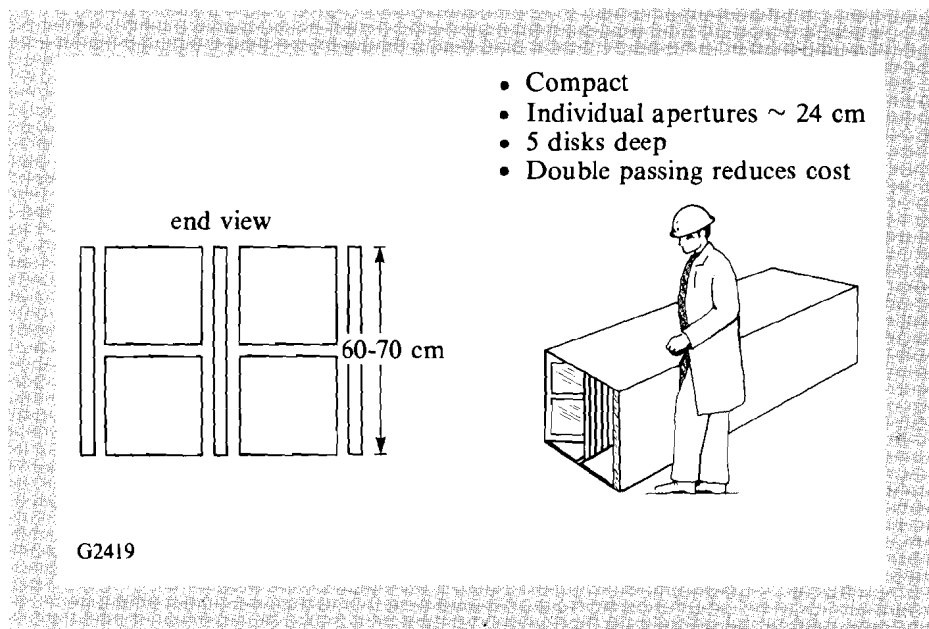


Fig. 38.12  
Proposed MSA amplifier for the OMEGA Upgrade. It will be a  $2 \times 2$  unit, 5 disks deep, and double passed.

parameterized in beam diameter. Since spatial filters and, consequently, propagation distance are relatively inexpensive compared to amplifier clear aperture, it is advantageous to use the maximum practical propagation distance. An upper limit of approximately 11 m is set by building-size limitations. Plan and elevation views of the proposed booster stage are shown in Fig. 38.13.

### Pulse-Shape Requirements

The OMEGA upgrade must be capable of producing a shaped pulse consisting of a long (5-ns), low-intensity “foot” smoothly transitioning into a short (0.5-ns), intense, main pulse. While the main-pulse shape is fixed, the shape of the foot pulse must remain flexible [3 ns to 5 ns (FWHM) containing 2 kJ to 6 kJ] in order to accommodate various target designs under consideration. The foot pulse has rapid turn-on (0.1 ns) followed by a smooth rise to a peak power that is  $\sim 4\%$ – $5\%$  of the main pulse. “Frozen-wave,” transmission-line-driven Pockel cells<sup>5</sup> are capable of generating the system input required for the foot. The main pulse contains 24 kJ of energy and is a simple truncated 0.55-ns to 0.75-ns FWHM Gaussian. The truncation point can vary but is envisioned to be at the 80% integrated energy time. Main-pulse truncation can be done at the main-pulse oscillator output using Si-switch-driven Pockel cells.

### Beam Modulation and Damage Fluences

The peak expected beam modulation, damage fluences, and fill factor, regardless of amplifier geometry, determine the clear apertures of the system. A 1.8:1 beam modulation is postulated for both the

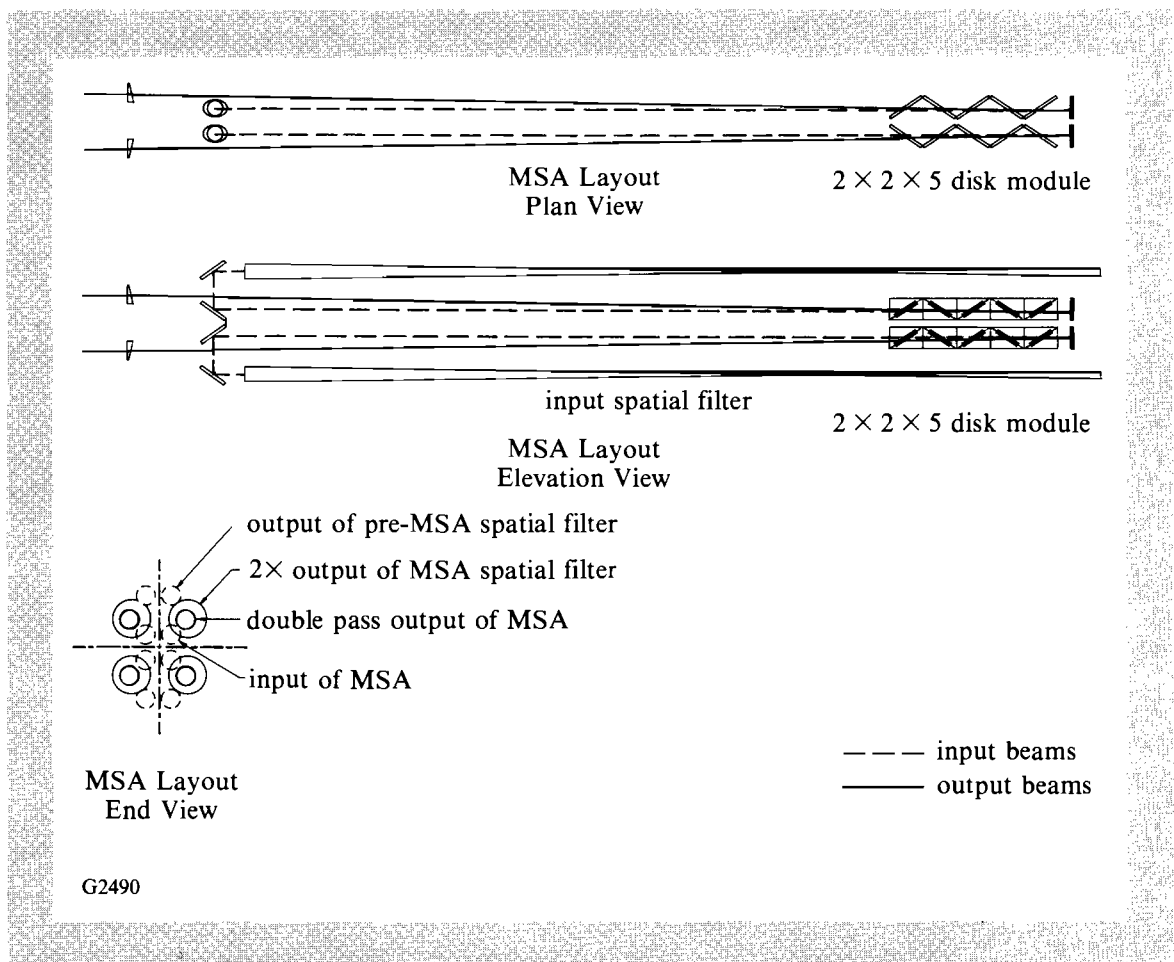


Fig. 38.13  
Plan and elevation views of the double-passed amplifier stage.

351-nm and 1054-nm final stages. This modulation is conservative with respect to the OMEGA<sup>6</sup> experience and comparable to experience elsewhere<sup>7</sup>. Calculations are underway to verify this modulation estimate.

Damage fluences are a function of the type of coating, the wavelength, and the pulse width. The greatest damage threat for the main pulse occurs at the shortest pulse width. Because of the sliding energy scale for the foot pulse, it is not as clear where the greatest damage threat for the foot pulse occurs. The energy requirement for the foot varies linearly with the pulse width. The damage fluence for AR-coated optics tends to vary as the square root of the pulse width at 1054 nm and the fourth root of the pulse width at 351 nm. Thus, the greatest damage threat for the foot occurs, counter-intuitively, at the longer pulse width. Since only AR coatings will be used in the frequency-converted subsystem and the beam size in this subsystem is constant, the most damage-threatened coating is the AR coating, which sees the greatest energy. For this system, this would be the AR coating on the output of the tripler.

In order to minimize the 1054-nm damage threat, the output of the final amplifier will go directly into an expanding spatial filter. The most-threatened, 1054-nm coating is on the input lens to this spatial filter. Because of the large decrease in damage fluences in going from 1054 nm to 351 nm, the final spatial filter will have a minimum magnification of 1.4.

Fused silica will be used exclusively for optics in the frequency-converted section. Because of the Pt-inclusion damage problem, any locations in the 1054-nm chain where the peak fluence exceeds  $0.75 \text{ J/cm}^2$  in the main pulse or  $3.75 \text{ J/cm}^2$  in the foot will also be fused silica.

The base-line type of Ar coatings at both 1054 and 351 nm is the Sol-Gel technology. The damage fluences for these coatings<sup>8</sup> are given in Table 38.I.

Table 38.I Sol-Gel AR damage fluences

1054 nm on fused silica		351 nm on KDP	
0.62 ns	10 $\text{J/cm}^2$	0.5 ns	3.8 $\text{J/cm}^2$
5.5 ns	15 $\text{J/cm}^2$	5.0 ns	6.8 $\text{J/cm}^2$

Note: Difference in pulse widths between 1054 and 351 nm is due to frequency conversion.

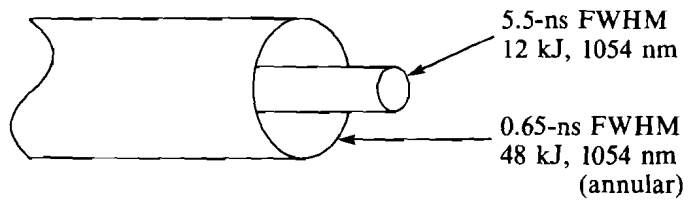
G2684

Using all of the above data and a postulated 80% fill factor, the minimum calculated clear aperture for the final amplifier is 17 cm for the main beam alone. The minimum calculated clear aperture for the foot beam is 6.2 cm. For a combined beamline where both pulses share the same 351-nm optics with a 70% fill factor, the minimum calculated clear aperture is 20 cm.

#### Coaxial Propagation: Co-propagation

Very early in the conceptual design of the upgrade it was realized that the 60 beams required for uniform target illumination presented a major beam-transport and beam-timing effort. Separate foot- and main-pulse beamlines doubled the difficulty. Propagating a shaped pulse through the laser system incurred an unacceptable conversion-efficiency penalty. The solution to this dilemma is to coaxially propagate the two beams. Figure 38.14 illustrates the concept. The foot pulse propagates as the inner beam and the main pulse propagates as the outer, annular beam. There is an antimixing zone between the two beams, accounting for 10% of the clear aperture area, to prevent interference effects between the two beams. The ratio of beam areas is 4.5:1 and the intensity ratio is 5.5:1 (main:foot). The two pulses are mixed on target by the DPP's located before each focus lens.

- Reduces transport optic cost and complexity by a factor of 2.



- An area ratio of 4.5:1 reduces the peak intensity ratio to 5.5:1.
- DPP's "mix" the two pulses on target.

G2485

Fig. 38.14  
Coaxial propagation: co-propagation.

Physical separation of the two beams allows optimization of the tripler thickness for both beams as shown in Fig. 38.15. The slower variation of  $3\omega$  damage fluences with temporal pulse width forces the two beams to operate at nearly the same fluence. Thus, there are only relatively minor differences in amplifier extraction between the two beams.

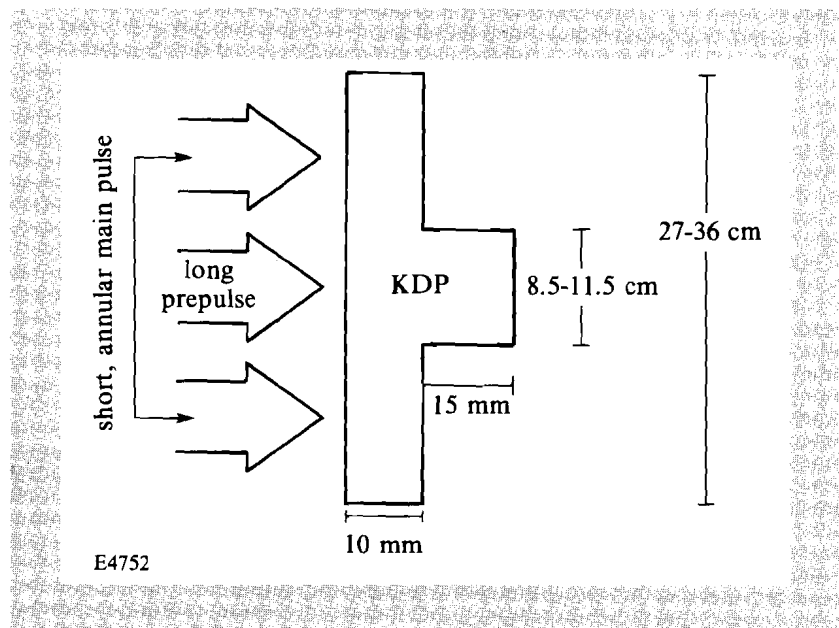
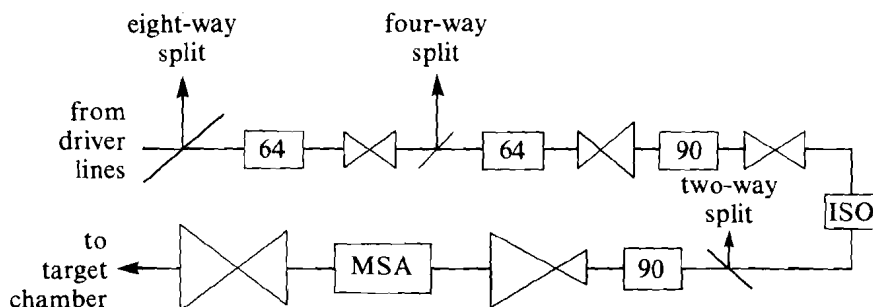


Fig. 38.15  
"Top hat" tripler shape allows efficient conversion of a co-propagated beam.

### 60-Beam Generation

The remaining problem is how to generate the 60 beams initially from the existing 24-beam system. Each of the 60 beams generated must have the same performance as the current 1054-nm OMEGA beamlines. Current OMEGA beamlines have produced over 200 J in a 0.8-ns pulse. It is desirable to perform the splitting at as small an aperture as possible to reduce costs and facilitate path-length equalization. The leading candidate staging is shown in Fig. 38.16. This staging, through the first 90-mm rod, is identical to the current OMEGA staging with the exception of the eight-way split being a six-way split.

Since the length of the chain has been increased and the small-signal gain has been correspondingly increased, provision has been made after the first 90-mm rod for the inclusion of active isolation to prevent chain self-oscillation. The need for isolation will be experimentally verified during the prototype phase.



G2514

Fig. 38.16

Proposed restaging of OMEGA to generate 60 beams which have the same performance as the existing beamlines.

The staging shown in Fig. 38.16 has several advantages that are not immediately apparent. The saturated gain of the final 90 is 4.3, which is more than adequate to overcome the two-way split and the loss associated with the isolator. This means that the first 90 and splitting region can operate at relaxed fluence levels. Further advantage can be taken of the available drive in this configuration by including a slight ( $\sim 5\%$ ) magnification in the relay between the 90's. This allows the majority of the rod system to operate at a reduced fill factor ( $\sim 75\%$ ) in order to reduce radial gain variations and avoid birefringent areas in the rods.

### Conclusion

A number of new ideas and emerging technologies have been coupled with proven laser designs to achieve a cost-effective upgrade to the OMEGA laser system. The novel multisegmented amplifier

concept has been coupled with double-passing for high efficiency, high extraction, and concomitant lower cost. Co-propagation, combined with distributed phase plates, provides a compact method of generating the high-dynamic-range,  $3\omega$  pulse required on target. Extensive use is made of 16,000-shot-proven OMEGA design hardware to drive the MSA. This combination of new technology and verified designs will allow generation of 60 beams, each with 500 J in the required temporal shape at 351 nm.

#### ACKNOWLEDGMENT

This work was supported by the U.S. Department of Energy Office of Inertial Fusion under agreement No. DE-FC03-85DP40200 and by the Laser Fusion Feasibility Project at the Laboratory for Laser Energetics, which has the following sponsors: Empire State Electric Energy Research Corporation, New York State Energy Research and Development Authority, Ontario Hydro, and the University of Rochester. Such support does not imply endorsement of the content by any of the above parties.

#### REFERENCES

1. 1983 Laser Program Annual Report, Lawrence Livermore National Laboratory, UCRL-50021-83, pp. 6-13 (1984).
2. LLE Review **19**, 123 (1984).
3. R. S. Craxton, "High Efficiency Tripling Schemes for High-Power Nd:Glass Lasers," *IEEE J. Quantum Electron.* **QE-17**, 1771 (1981).
4. 1985 Laser Program Annual Report, Lawrence Livermore National Laboratory, UCRL-50021-85, pp. 6-38 (1986).
5. J. F. Whitaker, T. B. Norris, G. Mourou, and T. Y. Hsiang, "Pulse Dispersion and Shaping in Microstrip Lines," *IEEE Trans. Microwave Theory Tech.* **MTT-35**, 41 (1987).
6. S. Skupsky, "A Source of Hot Spots in Frequency-Tripled Laser Light," LLE Review **31**, 106 (1987).
7. 1981 Laser Program Annual Report, Lawrence Livermore National Laboratory, UCRL-50021-81, pp. 2-35 (1982); J. T. Hunt, W. W. Simmons, D. R. Speck, W. E. Warren, and D. Eimerl, "Beam Propagation in the Frequency-Converted Subsystems of Nova and Novette," Lawrence Livermore National Laboratory, UCID-19086 (1981).
8. I. Thomas, "High Laser Damage Threshold Porous Silica Antireflective Coating," *Appl. Opt.* **25**, 1481 (1986).

## **Section 2**

# **ADVANCED TECHNOLOGY DEVELOPMENTS**

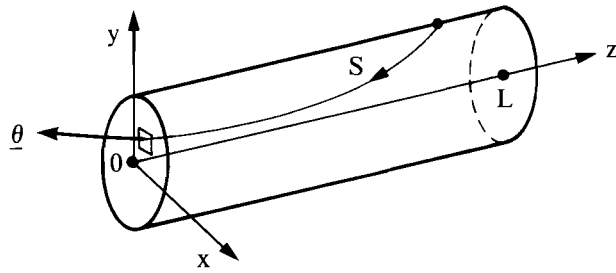
### **2.A CASER – A New Code for Calculating the X-Ray Laser Emission from Line-Focus Plasmas**

X-ray laser gain due to collisional excitation has been observed from exploding-foil targets at Lawrence Livermore<sup>1-3</sup> and from solid targets at NRL.<sup>4</sup> Crucial to the interpretation of both experiments is an understanding of x-ray refraction in the density profiles produced by line-focus irradiation.<sup>5</sup> In this article we describe a new code, CASER (combine amplified spontaneous emission with refraction), which solves the radiation-transport equation along all relevant three-dimensional (3-D) x-ray trajectories through a line-focus plasma, and performs whatever integrations of the emerging flux over space, angle, time, and frequency are necessary in order to replicate experimental observations. The capabilities of the code are illustrated with reference to exploding selenium foils irradiated under the conditions of Livermore x-ray laser experiments.<sup>1-3</sup> While its present application is to x-ray laser experiments, the code has a broader potential application to a wide range of radiation-emission problems from multidimensional plasmas.

The general problem addressed by the code is illustrated in Fig. 38.17, with respect to a line-focus plasma that is approximately cylindrical in shape. Under the Livermore conditions, the plasma would be a few hundred microns in diameter and up to 4 cm long. In

Fig. 38.17

Geometry for determining the radiation emitted from a line-focus plasma. The total emission from the surface at  $z = 0$  is the integral of the spectral intensity  $I_0$  over space  $(x,y)$ , angle  $(\theta_x, \theta_y)$ , frequency, and time.  $I_0$  is calculated by solving the radiation-transport equation (including a gain term) along each trajectory.



TC2413

order to determine the total energy ( $E_{\text{tot}}$ ) radiated across the exit surface at  $z = 0$ , it is necessary to perform the following multidimensional integral:

$$E_{\text{tot}} = \int I_0(x, y, \theta_x, \theta_y, \nu, t, L) \cos\theta dx dy d\theta_x d\theta_y d\nu dt . \quad (1)$$

The integrand  $I_0$  is the spectral intensity and has units  $\text{ergs}\cdot\text{cm}^{-2}\cdot\text{srad}^{-1}\cdot\text{freq}^{-1}\cdot\text{sec}^{-1}$ . It is assumed that all rays of interest emerge at small angles  $\theta$  to the surface normal, so that  $\cos\theta$  can be taken to equal unity. The integral is generally performed over the area of the exit surface in the  $x$ - $y$  plane as shown in the figure. However, it is sometimes necessary to increase the area of integration to include contributions from rays emerging from the curved edge of the plasma. The integral over angle  $(\theta_x, \theta_y)$  is dominated by the contributions of rays whose trajectories encompass all or most of the length of the plasma in the  $z$  direction. The quantity  $\theta_x$  is defined to be the cosine of the angle between the direction of the emerging ray and the  $x$  axis. For small angles from the surface normal,  $\theta_x$  is the angular deviation of the emerging ray from the  $z$  axis, measured in the  $x$  direction.

Integration over the spectral profile  $\Psi(\nu)$  is necessary because different portions of the spectrum see different gain in the plasma, and integration over time is required for all except time-resolved diagnostics. The spectral intensity  $I_0$  at the exit surface ( $z = 0$ ) is the solution of the radiation transfer equation

$$\frac{dI}{ds} = gI + \sigma \quad (2)$$

along the trajectory, integrated through a plasma of length  $L$ . (Corrections to this equation due to a spatially varying refractive index<sup>6</sup> are negligible in our application since the refractive index  $\mu \approx 1$ .)

In Eq. (2), the term  $\sigma$  represents spontaneous emission and a positive  $g$  signifies gain. (For most plasmas,  $g$  is negative and represents the opacity, corrected for stimulated emission.) For a spectral line, we can write  $g(\nu) = g_0 \Psi(\nu - \nu_0)$ , where  $\Psi$  gives the line shape [normalized so that  $\Psi(0) = 1$ ] and  $g_0$  gives the line-center gain. For the Livermore x-ray laser, we assume a Doppler line shape with width proportional to the square root of the ion temperature. We assume that  $g$  and  $\sigma$  share the same line shape.

The trajectories are calculated by integrating the 3-D ray equation,<sup>7</sup> simplified for the case of current interest where  $\mu \approx 1$  and the path length  $s \approx z$ :

$$\begin{aligned} \frac{d}{dz}(x,y) &= (\theta_x, \theta_y) \\ \frac{d}{dz}(\theta_x, \theta_y) &= \left( \frac{\partial \mu}{\partial x}, \frac{\partial \mu}{\partial y} \right) \\ \mu &= (1 - n_e/n_c)^{1/2}, \end{aligned} \quad (3)$$

where  $n_e$  is the electron-number density and  $n_c$  is the critical electron-number density corresponding to the x-ray wavelength ( $2.8 \times 10^{24} \text{ cm}^{-3}$  for 200 Å). Each trajectory is calculated backwards starting from the emerging point  $(x,y)$  and direction  $(\theta_x, \theta_y)$ , and terminating at  $z = L$  unless the ray first enters across the curved boundary (as occurs in Fig. 38.17 at point  $P$ ). If it is desired, the radiation-transport equation can then be integrated forward along the trajectory (i.e., in the direction of decreasing  $z$ ) for each frequency in the spectrum to include effects due to a spatially varying line shape. However, in some cases it is reasonable to assume that  $\sigma/g$  is independent of space and frequency; some computational time can then be saved by using the analytic solution<sup>5</sup> to Eq. (2) at the line center:

$$I_0 = \frac{\sigma}{g} (e^G - 1), \quad (4)$$

where

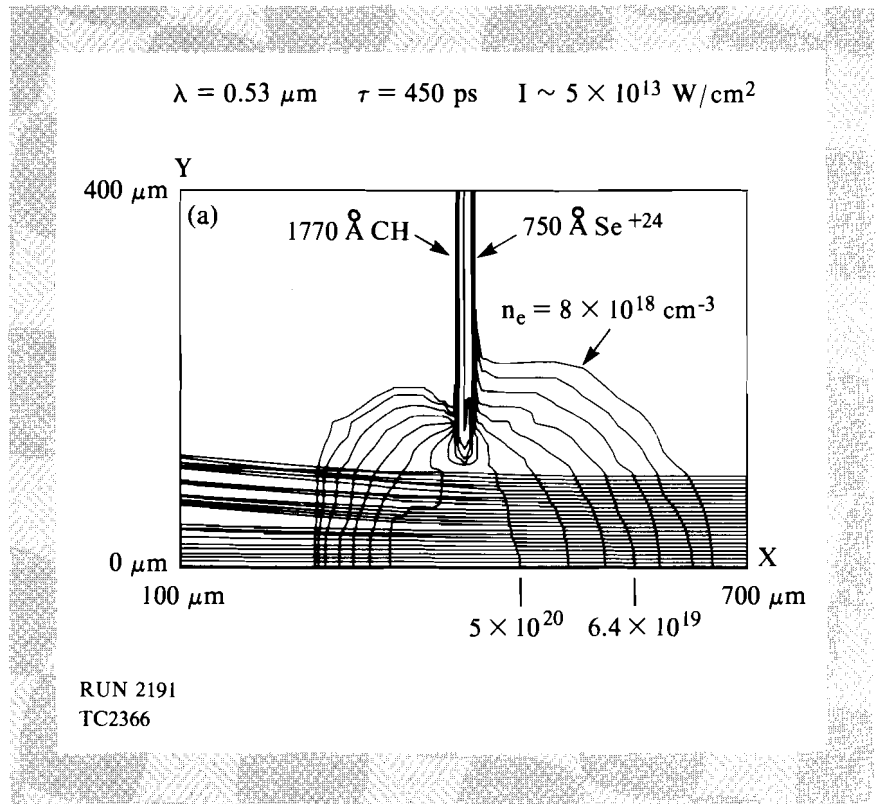
$$G = \int g dz. \quad (5)$$

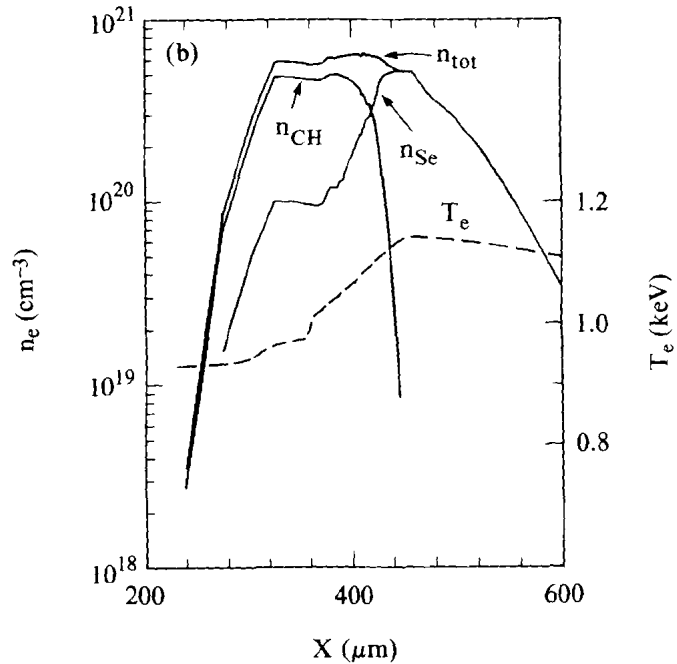
The frequency dependence of  $I_0$  can then be easily found since  $G$  has the same line shape as  $g$ .

It should be noted that CASER does not calculate the quantities  $n_e$ ,  $g$ , and  $\sigma$ . These need to be supplied from hydrodynamic and atomic-physics models. In the work presented here,  $n_e$  is obtained from a simulation using the two-dimensional (2-D) hydrodynamics code *SAGE*, and  $g$  and  $\sigma$  from an ad hoc model.

In order to illustrate its features, the code has been used as a postprocessor to a 2-D *SAGE* simulation of an exploding selenium foil, under conditions representative of the Livermore experiment reported in Refs. 1 and 2. The experiment (750 Å Se on 1500 Å of Formvar irradiated at  $5 \times 10^{13}$  W/cm<sup>2</sup>) was modeled using 750 Å of Se<sup>+24</sup> (perfect gas) on the CH thickness (1770 Å) equivalent to 1500 Å of Formvar. Representative density contours at the peak of the (optical) laser pulse are shown in Fig. 38.18(a). The laser is incident from the right and has just burned through the foil; the plasma extent is therefore greater on the right (selenium) side of the figure. The plasma is assumed symmetrical about the plane  $y = 0$ . Lineouts of electron density and temperature in this plane are shown in Fig. 38.18(b), including separate profiles for the CH and the Se. A problem with the current treatment of multiple materials in the Eulerian code *SAGE* is that separate equations are solved for each of the two densities, leading to some numerical diffusion. (The code contains no physical model for diffusion or mixing. The question of whether inter-material diffusion occurs to a significant extent in the experiment is not addressed here.) The extent of the numerical diffusion may appear to be exaggerated because the densities are plotted on a logarithmic scale; however, it is clear that the boundary between the two materials occurs just to the right of center, about 20 μm to the selenium side. This is consistent with the fact that, although the target initially contains 10% more selenium electrons (assuming neon-like ionization to Se<sup>+24</sup>), some of the selenium is ablated early in the interaction. In a comparison calculation using two-sided irradiation, the boundary appears a little to the left of center.

Fig. 38.18(a)  
*SAGE* simulation of an exploding CH/Se foil, for conditions corresponding to Livermore x-ray laser experiments. The foil is irradiated in line-focus geometry by a single beam, incident from the right in a 450-ps pulse of 532-nm light at  $5 \times 10^{13}$  W/cm<sup>2</sup>. Just after the laser burns through the foil a region of small density gradient is established near the center, allowing propagation of x rays through long distances in the z direction.





RUN 2191  
TC2400

Fig. 38.18(b)  
Lineouts of electron density and temperature along the  $x$  axis of Fig. 38.18(a), including individual densities of the CH and selenium components. In spite of some numerical diffusion of the two components into each other, the boundary between the two is approximately in the center of the profile.

In the CASER calculations presented here, the  $x$  rays are bent according to the gradients of total electron density  $n_e$ . A very simple ad hoc formula is used for the intrinsic line-center gain  $g_0$ :

$$g_0 = 1.25 \times 10^{-20} n_{Se}; \tag{6}$$

whenever the following three conditions are all satisfied: selenium must be the dominant material ( $n_{Se} > n_{CH}$ ), the inversion must not be destroyed by collisions ( $n_e < 10^{21} \text{ cm}^{-3}$ ), and the plasma must be sufficiently hot to be in the neon-like state ( $T_e \geq 300 \text{ eV}$ ). If any of these conditions are not satisfied,  $g_0$  is taken to be zero.

The exact position of the plastic/selenium interface is important because optimum x-ray lasing from long plasmas requires that the intrinsic gain be high in the central region of gentle electron density gradient. For the case of one-sided irradiation presented here, this requirement is clearly not met because the material in the center is plastic. For the case of two-sided irradiation the requirement is met, because the material in the center is selenium and the gain (assumed proportional to selenium density) is maximum there. This difference may partially explain the following experimental observation:

- (a) In the original NOVETTE experiments,<sup>1</sup> the signal up to a plasma length of 1 cm grew exponentially and was not greatly different for one- or two-sided irradiation;
- (b) In the same experiments,<sup>1</sup> the rate of growth of signal for one-sided irradiation fell off between 1 cm and 2 cm;
- (c) In later experiments on NOVA<sup>3</sup> with two-sided irradiation, exponential growth was maintained up to 4 cm.

However, the actual spatial and temporal dependence of the intrinsic gain  $g_0$  is far from certain. It has been inferred from experimental observations that  $g_0$  is low in the center for at least a significant portion of the disassembly time of the foil.<sup>3,5</sup>

Fig. 38.19

Ray trajectories used to perform the spatial integration (over  $x$  and  $y$ ) at one specific time (the peak of the pulse) and in one direction ( $\theta_x = 10$  mrad,  $\theta_y = 0$ ). Trajectories with values of  $y$  greater than  $20 \mu\text{m}$  are omitted for clarity. Gain exists in the plasma on the selenium side only ( $x \geq 420 \mu\text{m}$ ), and peaks at  $x \approx 450 \mu\text{m}$ . The integration algorithm selects those rays providing the dominant contributions.

In the integral of Eq. (1), the code typically integrates over all points  $x$  and  $y$  emerging in a specified direction. It can alternatively integrate over all angles  $\theta_x$  and  $\theta_y$  emerging from a specified point. In either case, just a small subset of possible rays provides the dominant contribution to the integral. This problem was recognized by London<sup>5</sup>; in order to obtain a convergent integral within reasonable computation time, it is necessary for CASER to select the most important rays automatically. How this is achieved is illustrated in Figs. 38.19 and 38.20.

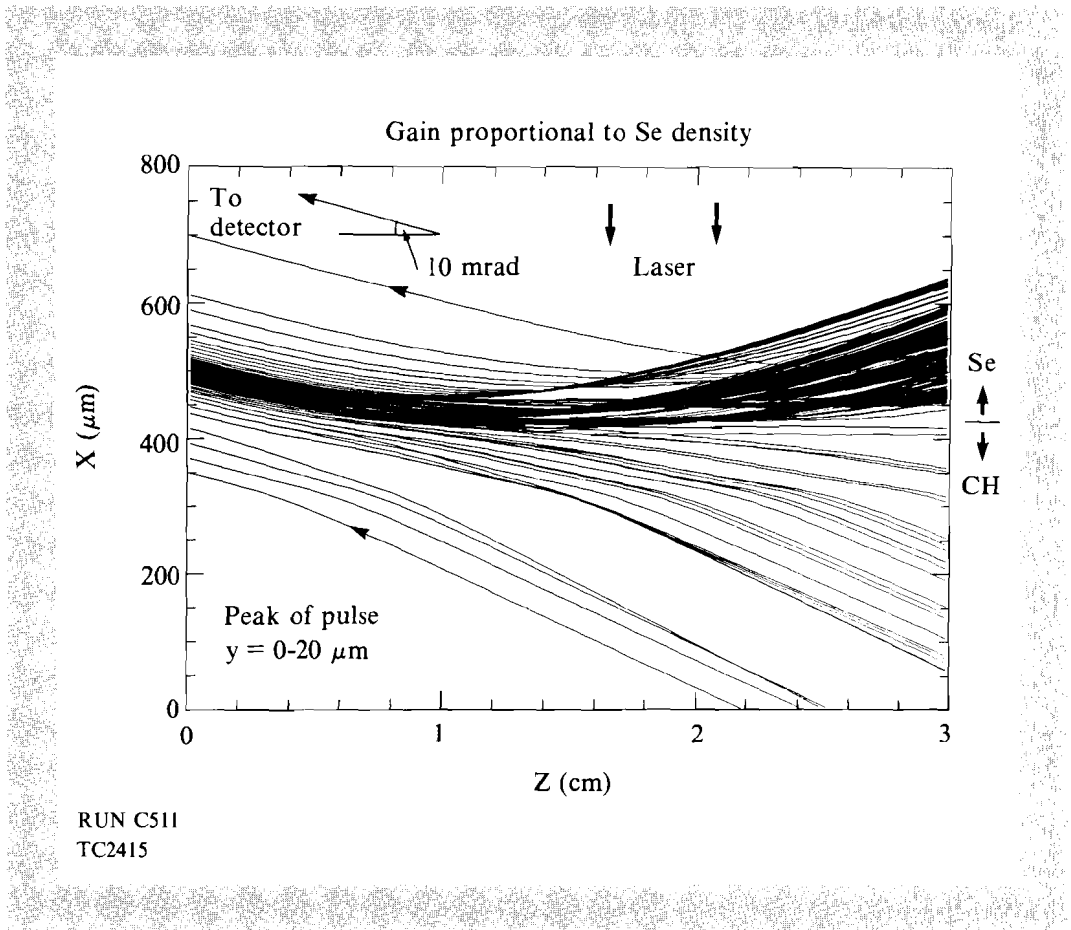


Figure 38.19 shows ray trajectories used in the integration through the profile of Fig. 38.18(a) to obtain the signal seen by a detector placed at 10 mrad to the  $z$  axis, for a plasma of 3-cm length. [Strictly speaking, it is the projection of the trajectories in the  $(x,z)$  plane that is shown.] Rays travel to the left, and emerge from the plasma at  $z = 0$  with an angle  $\theta_x$  of 10 mrad. The top half of the figure ( $y \geq 400 \mu\text{m}$ ) is selenium and contains all the gain. For clarity, the figure shows just those trajectories emerging with  $0 \leq y \leq 20 \mu\text{m}$ . The dominant rays emerge across a small portion of the exit surface at  $x \approx 500 \mu\text{m}$ , having experienced a turning point around  $x = 450 \mu\text{m}$  about halfway along the line focus. If gain were permitted on the CH side, we would observe a more symmetric clustering on the right-hand edge of the figure; i.e., at  $z = 3 \text{ cm}$ , the dominant rays would start with  $200 \leq x \leq 600 \mu\text{m}$  rather than with  $400 \leq x \leq 600 \mu\text{m}$ .

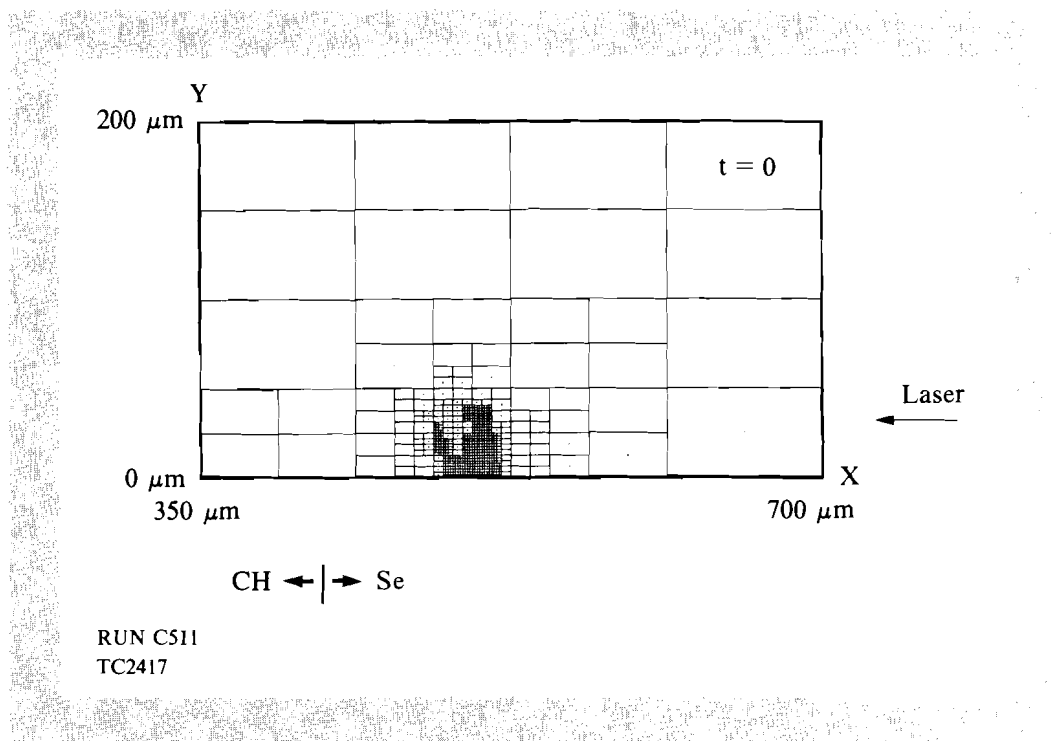


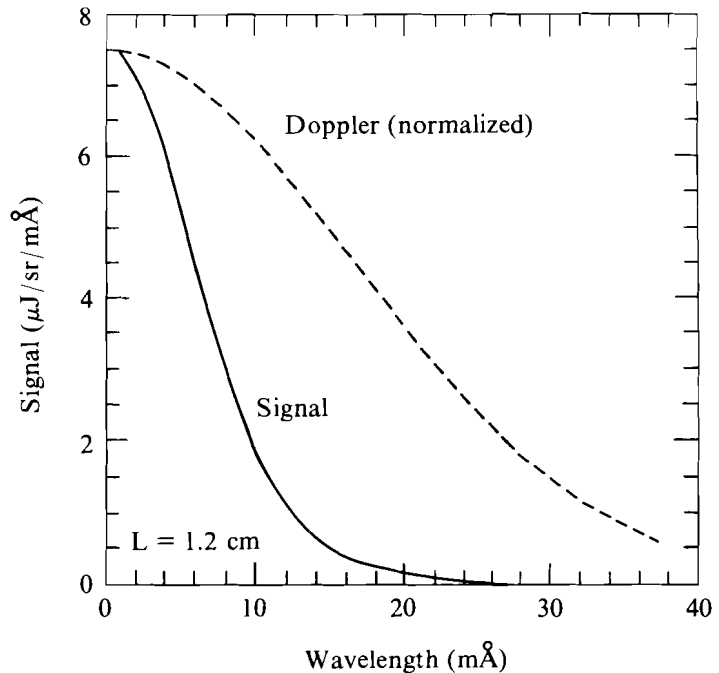
Fig. 38.20

Subdivision of the  $(x,y)$  plane corresponding to the trajectories of Fig. 38.19. Cells with large percentage contributions to the total integral have been successively subdivided. The dense portion indicates the small region responsible for the bulk of the gain.

Figure 38.20 shows how the  $(x,y)$  plane is successively subdivided during the integration. Cells with large fractional contributions to the total integral are subdivided into four smaller cells, whose contributions are then recalculated. Simpson's Rule in two dimensions is applied to each cell, necessitating trajectory computations at each cell center and corner. In order to avoid redundant trajectory computations, the integrand is actually a 2-D matrix of spectral intensities  $I_0$  corresponding to various frequencies and plasma lengths, with the subdivision pattern illustrated in Fig. 38.20 determined by the

largest element in the matrix (the line-center signal from the longest plasma length). The algorithm also necessarily includes means to ensure that if the region to one side of an interface is subdivided more than once, then the cell to the other side is subdivided regardless of its current contribution. The algorithm may be thought of as a numerical analog to a saddle-point integration. The large memory of the LLE Cyber 990 and its vector capability enable the integration to be performed efficiently.

The space- and time-integrated spectrum from a plasma of 1.2-cm length, as used in Ref. 1, is shown in Fig. 38.21 for a viewing angle  $\theta_x$  of 7 mrad (with  $\theta_y = 0$ ). The intrinsic (Doppler) profile, corresponding to the constant  $T_i = 500$  eV used for this calculation, is shown for comparison. (For this plasma, where  $T_i$  varies much slower spatially than  $g_0$ , a constant value of  $T_i$  is a reasonable approximation.) An inspection of the FWHM's of these two profiles indicates a narrowing by a factor of 2.9. This narrowing occurs because the line center experiences the strongest amplification. For an amplifier with a gain-length product  $G$ , it is easy to show that the narrowing factor is  $G^{1/2}$  in the limit of large  $G$ .<sup>8</sup> If we were to define an "average" intrinsic gain  $\bar{g}$  by equating  $(\bar{g}L)^{1/2}$  to 2.9, we would find  $\bar{g} = 7.0 \text{ cm}^{-1}$ , a value close to the experimentally inferred gain<sup>1</sup> of 5–6  $\text{cm}^{-1}$ . However, this procedure is not strictly justified since the spectrum of Fig. 38.21 does not correspond to a single intrinsic gain but is an integral over space and time.



RUN C511  
TC2418

Fig. 38.21  
Spectrum for a plasma of length 1.2 cm, integrated over space and time. Narrowing of the signal relative to the Doppler line profile intrinsic to the plasma is an indication of gain.

The most dramatic indication of x-ray lasing is seen when the signal, integrated over time, space, and wavelength, is plotted against plasma length (see Fig. 38.22). Here, the experimental points reported by Matthews *et al.* [Ref. 1, Fig. 4(a), two-sided illumination] are superposed for comparison. The calculation is normalized at 1.2 cm by an appropriate choice of  $\sigma/g$ . The factor  $1.25 \times 10^{-20}$  of Eq. (6) was chosen in order to provide a good fit to the data; a substantially poorer fit was obtained with this factor equal to  $1.0 \times 10^{-20}$ . The dashed and dotted curves of Fig. 38.22 are fits of the form  $\exp(\bar{g}L) \cdot (\bar{g}L)^{-1/2}$  used by Matthews *et al.*,<sup>1</sup> with  $\bar{g} = 5$  and  $6 \text{ cm}^{-1}$  respectively. The square-root term in this formula takes into account spectral narrowing; its origin is easy to understand since the integral over frequency is approximately the line-center gain times the width, and the width scales as  $(\bar{g}L)^{-1/2}$  in the limit of large  $\bar{g}L$ . However, use of this formula is not justified since similar square-root terms could arise

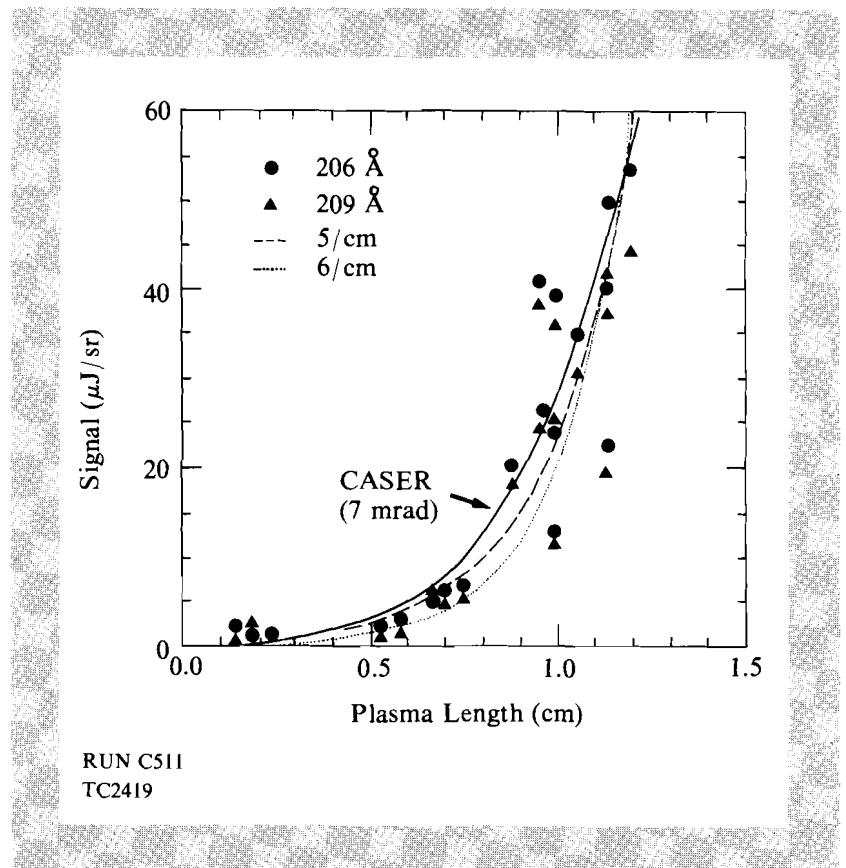


Fig. 38.22

Dependence of the integrated x-ray signal on plasma length. Simulation results (solid line) are compared with Livermore data for two lasing transitions. The dashed and dotted lines are fits to the Livermore data of form  $\exp(G)/G^{1/2}$ .

from the integrals over time and two spatial dimensions assuming (as is reasonable) that the gain is not uniform in space and time. Also, of course, the formula ignores refraction. A calculation such as is presented here is necessary to relate the gain inferred from observations integrated over time, space, and wavelength to the intrinsic gain in the plasma.

The angular dependence of the calculated signal, with respect to the angle  $\theta_x$  and for the greatest length used in Fig. 38.22 (i.e., 1.2 cm),

is shown in Fig. 38.23. The signal is seen to be quite peaked off-normal and strongly increasing from 0 to 10 mrad. This is due primarily to the selenium density (and therefore the intrinsic gain) falling off in the center of the plasma. A very similar curve to Fig. 38.23 was reported in Fig. 8 of Ref. 3, albeit for a 3-cm plasma and two-sided irradiation. It is possible that the large scatter in the experimental data seen in Fig. 38.22 for lengths around 1 cm is related to the strong dependence of signal on detector angle.

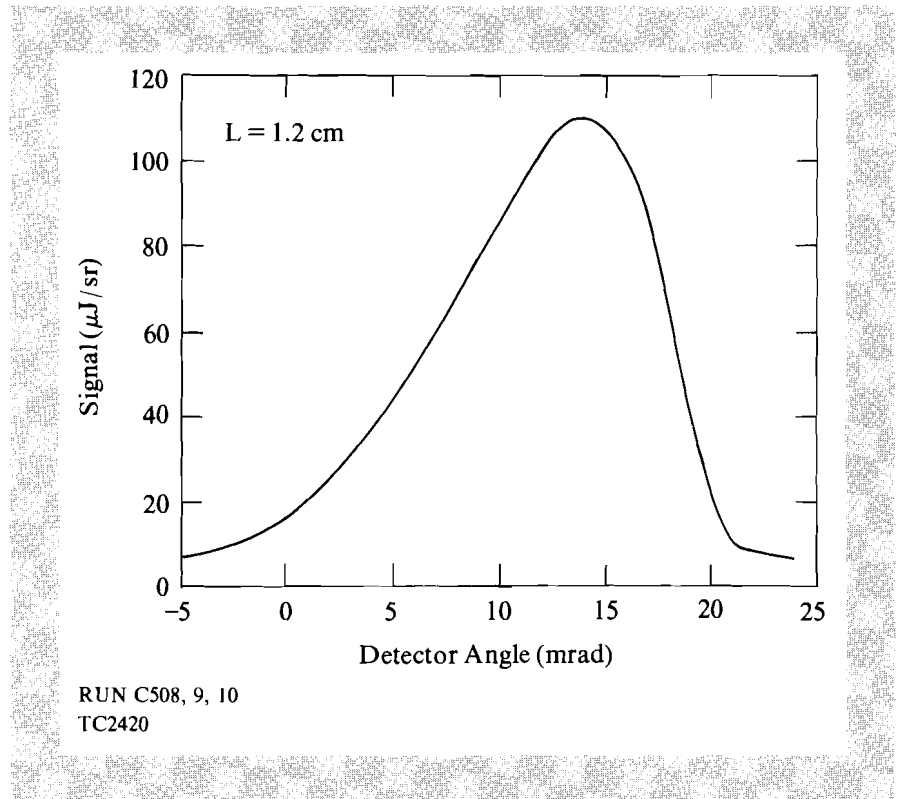


Fig. 38.23

Dependence of the integrated x-ray laser signal on the viewing angle  $\theta_x$  of the detector, for a 1.2-cm plasma. The peak at  $\theta_x = 13$  mrad is a consequence of the deficit of selenium in the center of the plasma.

Finally, the time evolution of the x-ray laser signal is shown in Fig. 38.24 for two viewing angles,  $\theta_x = 0$  and 7 mrad. As discussed, the signal at 7 mrad is the stronger signal. Both signals occur just before the peak of the driving laser pulse, with the 7-mrad signal peaking slightly earlier, qualitatively in agreement with Fig. 1 of Ref. 9. The FWHM's are 190 ps and 150 ps, respectively, somewhat less than the 290 ps observed in Fig. 3(a) of Ref. 1 for a 1-cm target displaying "moderate amplification," but consistent with the observation of Ref. 1 that the pulse width decreases with increased amplification.

In summary, the code CASER should prove useful in predicting experimental observations of x-ray lasing, given models of intrinsic gain within line-focus plasmas. The primary purpose of this article has

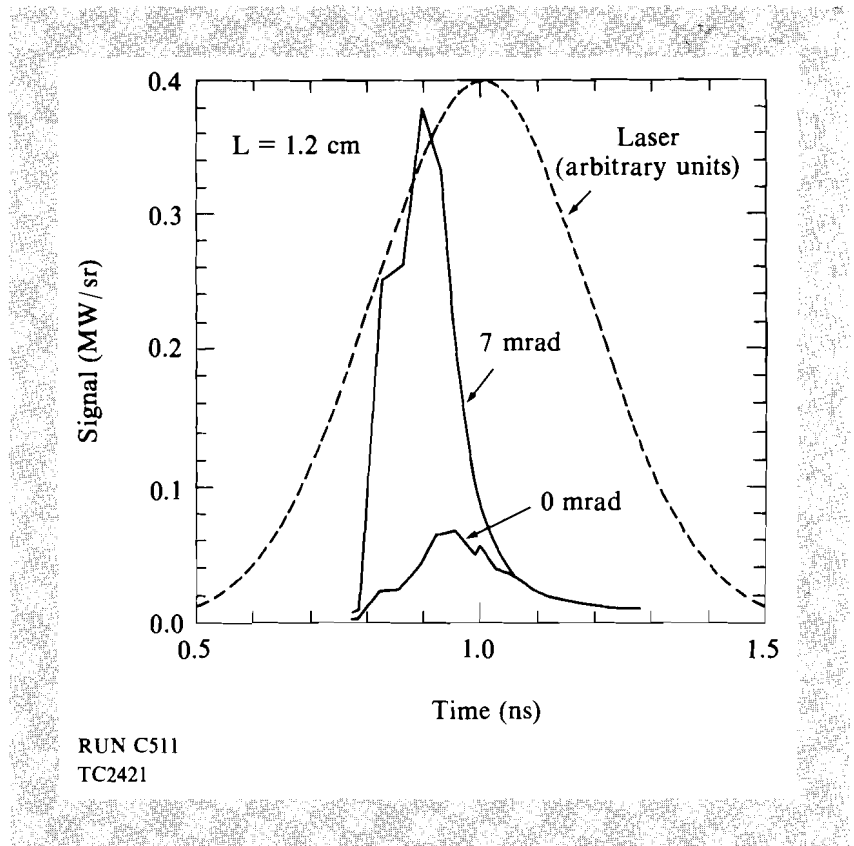


Fig. 38.24

Streaked x-ray laser emission from a 1.2-cm plasma, as viewed from two different directions. The 7-mrad signal emerges slightly earlier in time when refraction is more important. Later in time, when the density gradients have relaxed, there is no significant difference.

been to illustrate some of the capabilities of CASER. A more thorough analysis of the large data base of Livermore and NRL experiments is in progress, and depends in part on using a more realistic gain model. Given a reasonable gain model, the code will enable proposed new configurations for x-ray laser targets<sup>10</sup> to be evaluated and optimized with respect to refraction. This could permit useful gain to be obtained from lasers of modest energy.

#### ACKNOWLEDGMENT

This work was supported by the Laser Fusion Feasibility Project at the Laboratory for Laser Energetics, which has the following sponsors: Empire State Electric Energy Research Corporation, New York State Energy Research and Development Authority, Ontario Hydro, and the University of Rochester. Such support does not imply endorsement of the content by any of the above parties.

#### REFERENCES

1. D. L. Matthews *et al.*, *Phys. Rev. Lett.* **54**, 110 (1985).
2. M. D. Rosen *et al.*, *Phys. Rev. Lett.* **54**, 106 (1985).
3. D. Matthews *et al.*, *J. Opt. Soc. Am. B* **4**, 575 (1987).
4. T. N. Lee, E. A. McLean, and R. C. Elton, *Phys. Rev. Lett.* **59**, 1185 (1987).
5. R. A. London, *Phys. Fluids* **31**, 184 (1988).

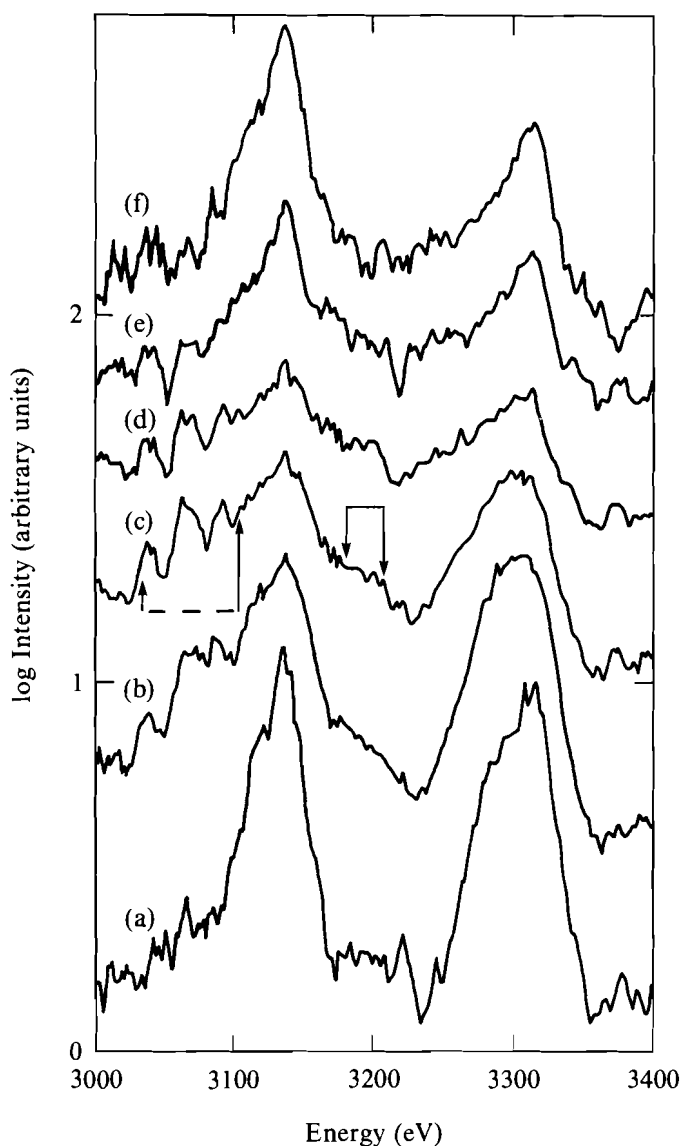
6. G. C. Pomraning, *The Equations of Radiation Hydrodynamics* (Pergamon Press, NY, 1973).
7. M. Born and E. Wolf, *Principles of Optics*, 5th ed. (Pergamon Press, Oxford, 1975), p. 122.
8. A. Yariv, *Quantum Electronics*, 2nd ed. (Wiley, New York, 1975), p. 285.
9. M. D. Rosen *et al.*, *Phys. Rev. Lett.* **59**, 2283 (1987).
10. D. Shvarts, B. Yaakobi, P. Audebert, T. Boehly, B. Boswell, D. Bradley, R. S. Craxton, R. Epstein, M. C. Richardson, and J. M. Soures, *X Rays from Laser Plasmas* (SPIE, Bellingham, WA, 1987), Vol. 831, pp. 283–292.

## 2.B Time-Resolved Spectroscopic Measurements of High Density in Ar-Filled Microballoon Implosions

In current high-density, laser-driven implosion experiments the determination of core conditions at stagnation is of great importance. This is particularly true of fusion experiments ( $D_2$ - or DT-filled targets) where nuclear diagnostics have been developed to estimate final core conditions.<sup>1,2</sup> A complementary approach, relying on x-ray spectroscopy of high- $Z$  gases (as total fill gas or as dopant), provides values of the electron density and temperature.<sup>3–6</sup> This technique has the added advantage that, with the inclusion of x-ray streak-camera technology, these parameters can be followed in time during the implosion. In addition to providing a valuable fusion diagnostic, this approach offers the opportunity to study the spectroscopy of many different highly stripped ions under extremely high-density conditions. In this article, we report time-resolved spectroscopic analysis of compressed, high- $Z$  gas-filled targets.

In a series of experiments supported by the NLUF, C. F. Hooper, D. P. Kilcrease, R. C. Mancini, and L. A. Woltz of the University of Florida, in collaboration with laboratory scientists, studied the implosion of Ar-filled plastic microballoons of dimensions  $420\ \mu\text{m} \times 6\ \mu\text{m}$  (diameter  $\times$  wall thickness).<sup>7</sup> These experiments used the 24-beam, UV ( $\lambda = 0.35\ \mu\text{m}$ ) OMEGA laser system, operated with the maximum illumination uniformity afforded by new distributed-phase-plate technology.<sup>8</sup> The total incident laser energy was 1700 J within a Gaussian pulse of duration  $680 \pm 50$  ps (FWHM). The targets were filled to pressures of 2 or 10 atm of Ar. A broad array of diagnostics,

including time-resolved, x-ray line spectroscopy with the SPEAXS curved crystal streak spectrograph<sup>9</sup> and time-integrated x-ray imaging of the compressed core, was deployed. Figures 38.25 and 38.26 show spectra recorded on two shots for different target pressures. The x-ray energy range shown covers emission from the  $\text{He}_\alpha$  and  $\text{Ly}_\alpha$  transitions of He- and H-like Ar and their associated satellite structure. Emission from the  $\text{He}_\beta$  and  $\text{Ly}_\beta$  lines was too weak for spectroscopic analysis (higher members of the helium and Lyman series either were not seen or lie beyond the energy range covered by the spectrograph). Spectra recorded from the implosion of an empty target were used to determine the extent of instrument-generated structure in the



E4712

Fig. 38.25

Series of time-resolved spectra for the 2-atm case. Spectrums (c) and (d) correspond to implosion stagnation.

(---) inner-shell transitions in C-, B- and Be-like Ar; (→) broad "blue satellite" feature. These spectra have been shifted vertically by arbitrary amounts for the purpose of suitable display in the same picture.

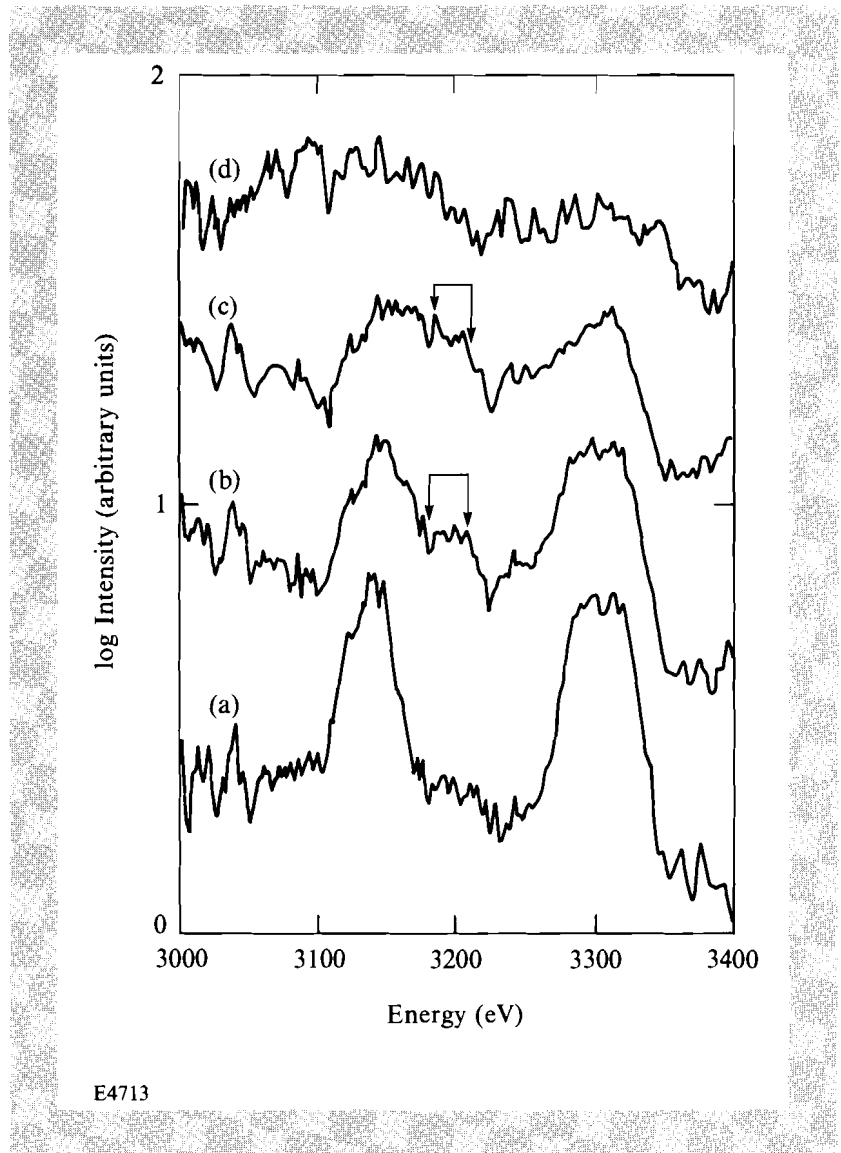


Fig. 38.26  
Same as in Fig. 38.25, but for the 10-atm case. In this case, spectrum (c) is characteristic of the stagnation. Note that after the stagnation (d), only continuum emission is seen.

continuum background. Figures 38.25 and 38.26 show time sequences of spectra obtained during the implosion. The He-like satellites ( $2l2l'-1s2l$ ) of  $\text{Ly}_\alpha$  are very intense and, together with the  $\text{Ly}_\alpha$  line, give rise to the spectral feature located around 3300 eV, whose low-energy side is dominated by satellite transitions and high-energy side by the  $\text{Ly}_\alpha$  line. Since the line shapes of the satellite and resonant transitions have been broadened sufficiently to cause merging, it is not possible to resolve the separate spectral features as was possible in previous implosion experiments.<sup>10-12</sup> As the implosion progresses, the overall shape of this composite spectral feature broadens further and shows varying degrees of asymmetry. While this line persists after the implosion for the low-pressure target (Fig. 38.25), only continuum emission is observed for the high-pressure target (Fig. 38.26). The spectral feature associated with the  $\text{He}_\alpha$  line and its Li-like satellites also shows an interesting evolution; as time advances we see the onset of an unusual emission feature ( $\sim 3160$  eV to 3220 eV) on the blue or

high-energy wing of the  $\text{He}_\alpha$  line in addition to the usual red satellites ( $1s2l2l' - 1s^22l$ ) found on the low-energy wing. This feature is observed in both Fig. 38.25 and Fig. 38.26. These broadened blue satellites achieve their highest intensity at the time of stagnation, when the maximum density is reached. For the target with the lower fill pressure, these features disappear when the system begins to decompress. A similar qualitative behavior has been observed in time-resolved spectra from other high-density implosion experiments.<sup>13</sup> In Fig. 38.25 we notice, between 3040 and 3100 eV, three emission peaks corresponding to the inner-shell transitions in C-, B- and Be-like argon. The evolution of their intensity can be observed before and at the implosion's stagnation. In Fig. 38.26 we see the red wing of the  $\text{He}_\alpha$  line partially truncated as the implosion approaches stagnation. We interpret this as an incipient absorption feature due to transitions in lower-ionization stages.

These spectra are compared to both Stark- and opacity-broadened theoretical line profiles to provide a history of the electron density and temperature during the implosion. The Stark-broadened line profiles, for different densities and temperatures, were computed for the  $\text{Ly}_\alpha$  line of H-like Ar and its He-like satellite transitions using a recently developed multielectron line profile code.<sup>14</sup> In previous spectroscopic diagnosis, based on analysis of He-like satellites of the  $\text{Ly}_\alpha$  line, the satellite line profile was approximated by a set of Lorentzian or Voigt

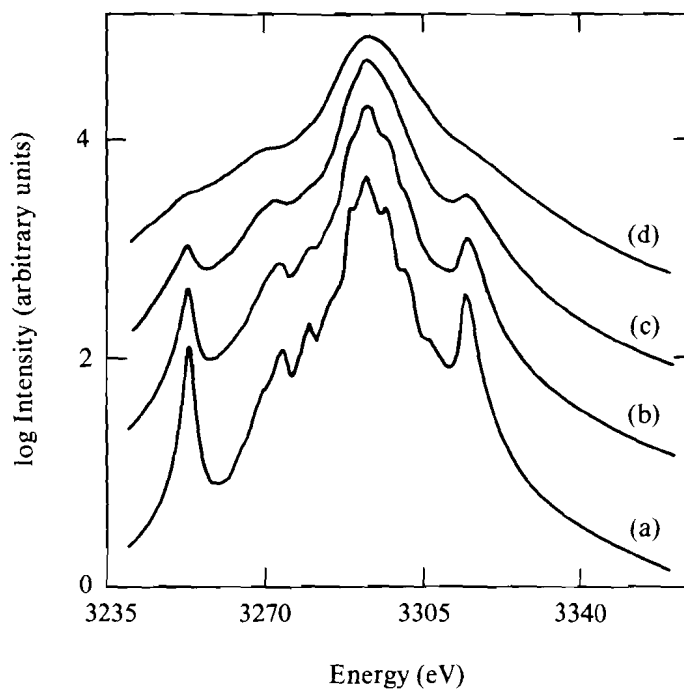


Fig. 38.27

He-like satellite line profiles for  $\text{Ar}^{+16}$  for an electron temperature  $T_e = 800$  eV and densities of  $N_e = 5 \times 10^{23}$  (a);  $1 \times 10^{24}$  (b);  $2 \times 10^{24}$  (c); and  $5 \times 10^{24}$  (d) in  $\text{cm}^{-3}$ .

E4714

line profiles whose individual widths were determined by instrumental broadening. However, we find that as the density increases, Stark-broadening and field-mixing effects become more important and can introduce substantial changes to the Voigt satellite line shapes. For example, in Fig. 38.27, we show a series of Stark-broadened satellite line profiles computed for increasing values of the electron density. The calculation involves all the transitions between the He-like double-excited  $2l2l'$  states, the relative distribution population assumed to be in local thermodynamic equilibrium (LTE), and the single-excited  $1s2l$  states. The Stark broadening is treated by the Smith-Hopper relaxation theory with the static ion approximation.<sup>10</sup> The relative distribution of population among doubly excited states was taken to be in LTE. As the density increases, the line shape loses the detailed structure that reflects the set of transitions involved in its calculation and turns into a rather broad and smooth line profile. Yet, at higher densities, the features of the shape still resemble the broad characteristics of the profile at low density (see Fig. 38.27). The fitting of the spectral feature associated with the  $Ly_\alpha$  line and its related satellite emission is done using an intensity model that combines the calculated line profiles of satellite and resonance transitions. Opacity broadening is simulated in each line profile by means of the uniform slab model and is characterized by the optical thickness at line center  $\tau_{os}$  (satellite) and  $\tau_{or}$  (resonance).<sup>10</sup> Doppler and instrumental broadening are also included. Before the experimental spectra are compared with the theoretical calculations, the continuum background, estimated from the spectrum over a broader range, is subtracted from the data. For a given spectrum and value of the electron density  $N_e$ , we pick  $\tau_{or}$  and  $\tau_{os}$  for the best possible fit to the experimental data; this is done automatically by a program that minimizes the sum of the square differences between experimental and theoretical (log intensity) points ( $Q^2$ ). This procedure is repeated for different values of  $N_e$  allowing us to see the changes in  $Q^2$  and the values of  $\tau_{or}$  and  $\tau_{os}$  as a function of  $N_e$ . We find for each spectrum that there is a range of  $N_e$  over which  $Q^2$  has a minimum and the quality of the fit is very good. Next, the ratio of optical thickness  $\tau_{or}/\tau_{os}$ , obtained from  $Q^2$  multiplication, can be checked for consistency with the values computed using kinetic modeling. This ratio minimizes any uncertainty in the assumption of a characteristic geometrical length and is proportional to the ratio of populations in the lower state of each transition (ground-state H-like Ar and first, single-excited state in He-like Ar). Independently, a collisional-radiative kinetic code was also used to compute this ratio.<sup>14</sup> We have, therefore, examined the sensitivity of this ratio to different modeling assumptions such as optically thin, optically thick, LTE, or changes in the number of excited states. For electron densities above  $1 \times 10^{24} \text{ cm}^{-3}$  this ratio is rather insensitive to modeling details and becomes a function of only  $N_e$  and  $T_e$ . This is because at these high densities the  $n = 2$  level of He-like Ar gradually comes into LTE with the ground state ( $n = 1$ ) of H-like Ar, although, for example, this level is not in LTE with the  $n = 2$  level of H-like Ar. Comparison with kinetic calculations also lets us estimate values of the electron temperature  $T_e$ . An analysis of the data in Figs. 38.25 and 38.26, based on the above procedure, allows us to infer  $N_e$  and  $T_e$ . Table 38.II summarizes our findings.

Table 38.II Density and temperature results for the analysis of data in Figs. 38.25 and 38.26. Time is measured with respect to the peak of the laser pulse ( $1 \times 10^{24} \text{ cm}^{-3} \sim 4 \text{ g/cm}^3$ )

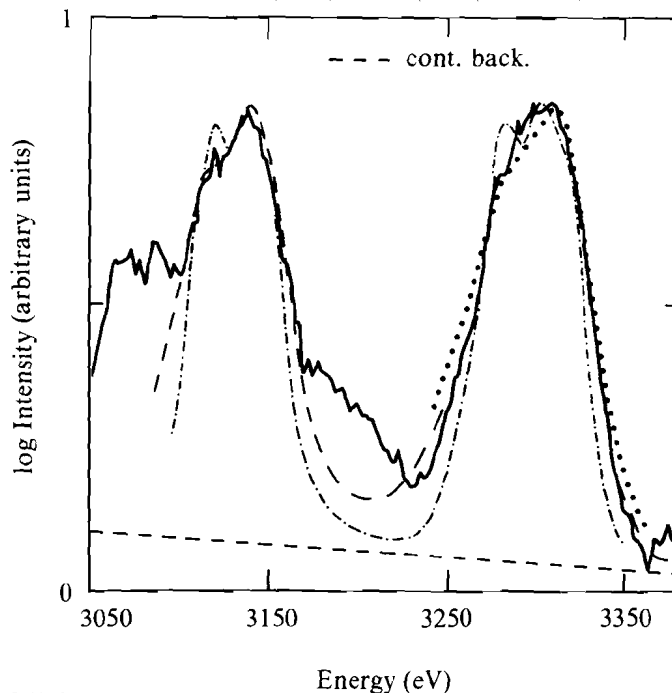
Figure Spectrum	Time Interval (ps)	Electron Density ( $\text{cm}^{-3}$ )	Temperature (eV)
1, (a)	109-171	$4.0-6.0 \times 10^{24}$	600-900
1, (b)	171-233	$4.0-6.0 \times 10^{24}$	600-900
1, (c)	202-264	$4.0-7.0 \times 10^{24}$	600-800
1, (d)	233-295	$6.0-8.0 \times 10^{24}$	500-600
1, (e)	295-357	$2.5-6.0 \times 10^{24}$	450-600
1, (f)	357-419	$2.5-4.0 \times 10^{24}$	450-600
2, (a)	312-375	$5.0-7.0 \times 10^{24}$	600-900
2, (b)	348-405	$3.0-6.0 \times 10^{24}$	600-800
2, (c)	375-427	$6.0-8.0 \times 10^{24}$	500-800

E5096

A similar analysis of the spectral feature associated with the  $\text{He}_\alpha$  line and its Li-like satellite transitions was performed and provides consistent results. An example of the level of agreement between the theoretical fits and the experimental line profiles of both the  $\text{He}_\alpha$  (3100-3170 eV) and  $\text{Ly}_\alpha$  (3260-3340 eV) spectral features is illustrated in Fig. 38.28. As can be seen for this particular spectrum, the best fit to both features corresponds to that computed for an electron density of  $5 \times 10^{24} \text{ cm}^{-3}$ . The continuum background level is also shown. We estimate that effects of temperature and density gradients can introduce uncertainties of less than 50% in our density inferences.<sup>15</sup>

It is important to note that the values of  $\tau_{\text{or}}$  (5-20), deduced in the fitting procedure, are significantly smaller than those required to fit the spectra from previous experiments.<sup>10,11</sup> Before stagnation we find  $\tau_{\text{or}} > \tau_{\text{os}}$ , while at, and after, stagnation  $\tau_{\text{or}} \lesssim \tau_{\text{os}}$ . One-dimensional hydrodynamic simulations of these experiments indicate that close to stagnation a central region of about 25% of the Ar mass is sufficiently hot to populate the *K*-shell ions, while the remaining Ar has a temperature in the range 200 eV to 600 eV.<sup>15,16</sup> Ionization balance calculations performed in this temperature range for densities greater than  $4 \text{ g/cm}^3$  indicate that the C-, B-, Be-, and Li-like ions share almost all the population and that the population of excited states becomes comparable to, or even exceeds, that for the ground states.<sup>17</sup> These results support the finding of a low opacity effect on resonant transitions and increases the likelihood of opacity effects on satellite transitions.

The analysis of the time-integrated, x-ray pinhole (2 keV to 4 keV), images of the compressed core, showing a spherically imploded Ar



E4968

Fig. 38.28

An example of the fittings obtained. This case corresponds to spectrum (b) in Fig. 38.25. Experimental spectrum (—); fitting (---).  $N_e = 1 \times 10^{24}$  (-·-·-·-·-);  $5 \times 10^{24}$  (---); and  $8 \times 10^{24}$  (·····) in  $\text{cm}^{-3}$ .

plasma of 35- $\mu\text{m}$  diameter, is also in reasonable agreement with our spectroscopic analysis. Assuming mass conservation, this would indicate average mass densities of 20 to 40  $\text{g}/\text{cm}^3$ .

In conclusion, the electron densities recorded here are the largest observed directly through spectroscopic means. Furthermore, the low opacity of the resonance lines, which is consistent with our modeling, implies the existence of radiation "windows" in very dense, hot plasmas. Since the spatial extent of the excited-state orbitals at these densities is comparable to the average interatomic spacing, the onset of the blue satellite features may indicate the initiation of a plasma-solid phase transition.<sup>18</sup> However, additional analysis is required to verify this speculation.

#### ACKNOWLEDGMENT

This work was supported by the U.S. Department of Energy Office of Inertial Fusion under agreement No. DE-FC03-85DP40200 and by the Laser Fusion Feasibility Project at the Laboratory for Laser Energetics, which has the following sponsors: Empire State Electric Energy Research Corporation, New York State Energy Research and Development Authority, Ontario Hydro, and the University of Rochester. Such support does not imply endorsement of the content by any of the above parties.

## REFERENCES

1. S. Skupsky and S. Kacenjar, *J. Appl. Phys.* **52**, 2608 (1981).
2. E. G. Gamalii, S. Yu. Gus'Kov, O. N. Krokhin, and V. B. Rozanov, *JETP Lett.* **21**, 70 (1975).
3. B. Yaakobi *et al.*, *Phys. Rev. Lett.* **39**, 1526 (1977).
4. K. B. Mitchell *et al.*, *Phys. Rev. Lett.* **42**, 232 (1979).
5. J. M. Auerbach *et al.*, *Phys. Rev. Lett.* **44**, 1672 (1980).
6. A. Hauer *et al.*, *Phys. Rev. Lett.* **45**, 1495 (1980).
7. C. F. Hooper, D. P. Kilcrease, R. C. Mancini, L. A. Woltz, D. K. Bradley, P. A. Jaanimagi, and M. C. Richardson, *Phys. Rev. Lett.* (to be published).
8. LLE Review **33**, 1 (1987).
9. B. L. Henke and P. A. Jaanimagi, *Rev. Sci. Instrum.* **56**, 1537 (1985).
10. N. D. Delamater, C. F. Hooper, Jr., R. F. Joyce, L. A. Woltz, N. M. Ceglio, R. L. Kauffman, R. W. Lee, and M. C. Richardson, *Phys. Rev. A* **31**, 2460 (1985).
11. N. D. Delamater, C. F. Hooper, Jr., M. C. Richardson, P. Jaanimagi, R. L. Kauffman, J. Scofield, L. A. Woltz, and T. Garber, *Phys. Rev. A* (in press).
12. C. F. Hooper, Jr., R. C. Mancini, D. P. Kilcrease, L. A. Woltz, M. C. Richardson, D. K. Bradley, and P. A. Jaanimagi, *SPIE* **913**, 129 (1988).
13. R. L. Kauffman (private communication).
14. L. A. Woltz and C. F. Hooper, Jr., *Phys. Rev. A* **38**, 4766 (1988).
15. R. C. Mancini and C. F. Hooper, Jr., *J. Phys. D* **21**, 1099 (1988).
16. J. Delettrez (private communication).
17. Y. T. Lee, *J. Quant. Spectros. & Radiat. Transfer* **38**, 131 (1987).
18. S. M. Younger, A. K. Harrison, K. Fujima, and D. Griswold, *Phys. Rev. Lett.* **61**, 962 (1988).

## Section 3

# NATIONAL LASER USERS FACILITY NEWS

During the second quarter of FY89 NLUF activity consisted of supporting future experiments on the GDL laser, the determination of the new deadlines for submission of FY90 proposals, a steering committee meeting, and notification of principal investigators. These activities should make it easier for current and future investigators to conduct their experiments smoothly. The changes to the proposal process will allow the Department of Energy San Francisco Office (DOE/SFO) to fund approved experiments at the beginning of the appropriate fiscal year.

**R. Whitlock** from NRL visited LLE to start planning for his experiment on GDL. This experiment will measure the effect of high-fluence x rays incident on a single crystal. The experiment is being done in collaboration with **J. Wark** and will use the GDL laser as the source of x rays. The x rays will be used to generate shock waves in the crystal and to probe the effect of these shock waves on the crystalline properties. This initial visit was meant to familiarize the visiting scientists with the GDL target chamber and operations. A final review of the experiment will be conducted when the planning is completed. The experiment will be scheduled for GDL time after the final review.

On 17 February 1989, **J. Krupa** and **E. Schalin** from DOE/SFO visited LLE. The NLUF proposal process was discussed and a preliminary schedule for the proposal process was completed. The

current deadline for submission of FY90 proposals to DOE/SFO will be 31 May 1989. The proposals will be sent to LLE for review by the NLUF Steering Committee. The recommendations of the steering committee will be sent to DOE. They will then notify the principal investigators who submitted proposals as to the results of the selection process. Thus, many of the administrative functions will shift to DOE allowing the LLE office to concentrate on the technical aspects of the NLUF program. This should provide better support for both administrative and technical problems encountered by scientists doing experiments at LLE. DOE/SFO will handle the announcements and call for NLUF proposals.

#### ACKNOWLEDGMENT

This work was supported by the U.S. Department of Energy Office of Inertial Fusion under agreement No. DE-FC03-85DP40200.

## Section 4

# LASER SYSTEM REPORT

### 4.A GDL Facility Report

During the second quarter of FY89, laser time in GDL was split between maintenance and interaction experiments in the Beta target facility. In addition, the GDL operation and engineering staff spent a portion of their time in support of OMEGA during part of the experimental program. The experiments concentrated on the effects of early-time transmission of laser light through fusion targets.

X-ray laser experiments were also conducted during this quarter. Work continued on the collisional excitation laser in germanium; for this study a polarizer and quarter-wave plate assembly was installed in the GDL beam to allow for the infrared irradiation of targets. GDL now has the capability to irradiate targets with any of three wavelengths: 1054 nm, 527 nm, or 351 nm. In addition, experiments were conducted on the photo-resonant pumping of Li-like iron with the H-like  $Ly_{\alpha}$  of aluminum.

The various maintenance tasks performed included oscillator alignment, oscillator etalon-change/pulse-width studies,  $q$ -switch studies, and the replacement of the existing  $q$ -switch device. Work was also carried out on the oscillator mode-locker, including the installation of flow meters, fine tuning the mode-locker, and studies relating mode-locker performance to pulse width.

A summary of GDL operations this quarter follows:

Beta Shots	
Pointing	36
XRL/Focus Study	31
Shine-through	175
Laser and Crystal Tuning	<u>93</u>
TOTAL	335

#### ACKNOWLEDGMENT

This work was supported by the U.S. Department of Energy Office of Inertial Fusion under agreement No. DE-FC03-85DP40200 and by the Laser Fusion Feasibility Project at the Laboratory for Laser Energetics, which has the following sponsors: Empire State Electric Energy Research Corporation, New York State Energy Research and Development Authority, Ontario Hydro, and the University of Rochester. Such support does not imply endorsement of the content by any of the above parties.

## 4.B OMEGA Facility Report

During this quarter, laser operations completed the implementation of SSD on OMEGA. Integrating several new technologies and converting the main laser to broadband operation has given much-improved, on-target intensity distributions. In addition, progress continued in power balancing all of OMEGA's 24 UV beams. Using a new cw ratiometer system, characterization of transport optics can now be accomplished to a much higher accuracy than has been previously achieved. Finally, the experimental programs of high-density and high-yield implosions have been supported by target shots with power-balanced SSD beams.

The concept of bandwidth generation and dispersion for frequency conversion, combined with distributed phase for the SSD effect, was first demonstrated on OMEGA on 12 January 1989. The impact of SSD on the main portion of the laser system was minimal, requiring less than two weeks to implement. Conversion of broadband light required the addition of two holographic diffraction gratings and an electro-optic bandwidth modulator to the low-energy portion of the driver line. The main amplifier chains did not require any modifications other than a minor adjustment to the spatial filter pinhole

sizes. Many shots were taken for diagnosis of temporal and spatial profile characterization followed by and mixed in with target experiments.

Further improvement in laser performance has come with the advent of a new laser-transport diagnostic. The transmission characteristics of the seven UV optics after frequency conversion can now be measured to within  $\pm 0.3\%$ . This is accomplished by sequentially injecting a full-aperture, cw, 351-nm laser into each beamline after the frequency-conversion crystals and measuring the overall transmission at the center of the target chamber. A schematic of the OMEGA transport integrating sphere (OTIS) system appears in Fig. 38.29.

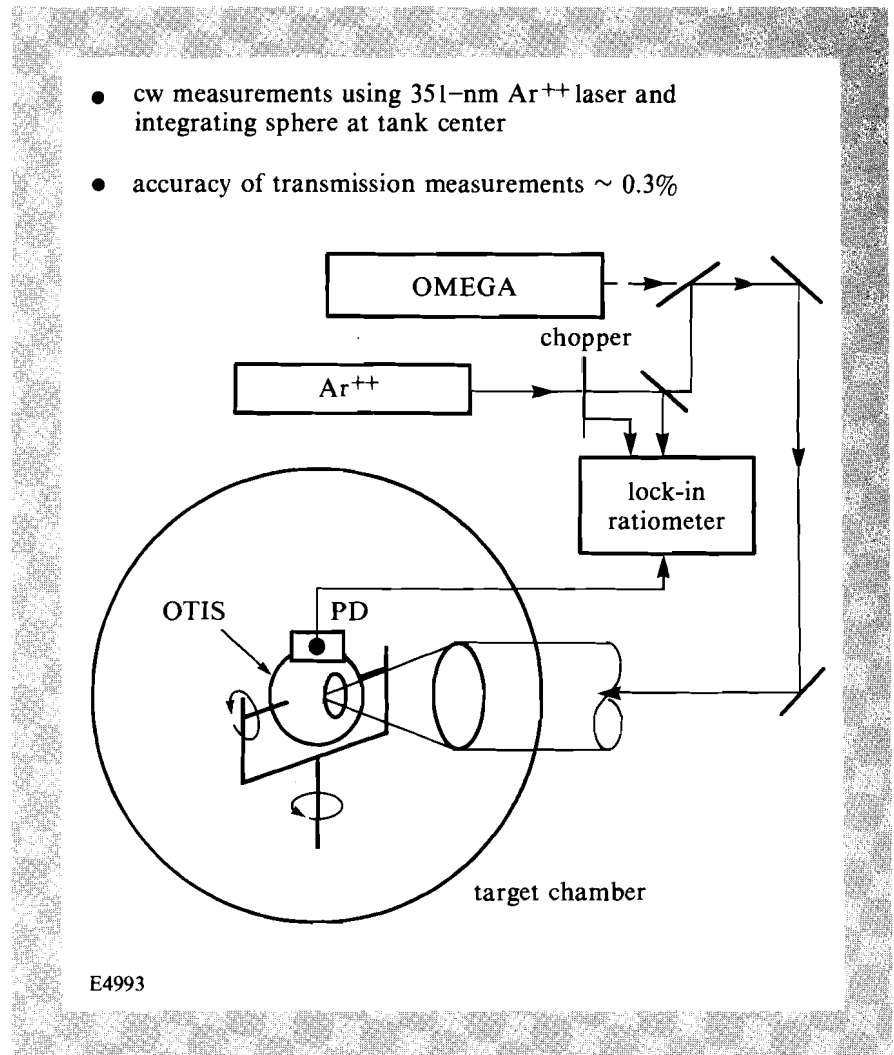


Fig. 38.29

The optical transmission at  $0.35\ \mu\text{m}$  of each OMEGA beamline is characterized by means of the OMEGA transport integrated sphere (OTIS)—a compact, remotely controlled integrating sphere located at the center of the OMEGA vacuum system. A  $0.35\text{-}\mu\text{m}$  Ar<sup>++</sup> laser, co-aligned to the OMEGA beams, provides the laser illumination for this measurement. The overall accuracy of the transmission measured with OTIS is  $\pm 0.3\%$ .

A synopsis of laser shots for this quarter follows:

Software	59
Driver	169
Laser	272
Target	<u>226</u>
TOTAL	726

#### ACKNOWLEDGMENT

This work was supported by the U.S. Department of Energy Office of Inertial Fusion under agreement No. DE-FC03-85DP40200 and by the Laser Fusion Feasibility Project at the Laboratory for Laser Energetics, which has the following sponsors: Empire State Electric Energy Research Corporation, New York State Energy Research and Development Authority, Ontario Hydro, and the University of Rochester. Such support does not imply endorsement of the content by any of the above parties.

# PUBLICATIONS AND CONFERENCE PRESENTATIONS

## Publications

R. Epstein, "The Design and Optimization of Recombination Extreme-Ultraviolet Lasers," *Phys. Fluids B* **1**, 214–220 (1989).

T. B. Norris, X. J. Song, W. J. Schaff, L. F. Eastman, G. Wicks, and G. A. Mourou, "Tunneling Escape Time of Electrons from a Quantum Well Under the Influence of an Electric Field," *Appl. Phys. Lett.* **54**, 60–62 (1989).

J. C. Lee, A. Schmid, and S. D. Jacobs, "Effects of Anchoring Under Intense Optical Fields in a Cholesteric Liquid Crystal," *Mol. Cryst. Liq. Cryst.* **166**, 253–265 (1989).

O. Barnouin, B. Yaakobi, J. Delettrez, R. Epstein, P. Jaanimagi, and L. M. Goldman, "Experimental and Numerical Study of Thermal Transport in 24-Beam Ultraviolet Irradiation of Spherical Targets," *J. Appl. Phys.* **65**, 969–977 (1989).

K. Meyer, M. Pessot, G. Mourou, R. Grondin, and S. Chamoun, "Subpicosecond Photoconductivity Overshoot in Gallium Arsenide Observed by Electro-Optic Sampling," *Appl. Phys. Lett.* **53**, 2254–2256 (1988).

M. Pessot, J. Squier, P. Bado, G. Mourou, and D. J. Harter, "Chirped Pulse Amplification of 300 fs Pulses in an Alexandrite Regenerative Amplifier," *IEEE J. Quantum Electron.* **25**, 61–66 (1989).

S. H. Chen and Y. F. Maa, "A Reexamination of the Synthesis of Liquid Crystalline Side-Chain Polyacrylates via Liquid-Liquid Phase Transfer Catalysis," *Macromolecules* **21**, 904 (1988).

- R. L. Berger, E. A. Williams, and A. Simon, "Effect of Plasma Noise Spectrum on Stimulated Scattering in Inhomogeneous Plasma," *Phys. Fluids B* **1**, 414-421 (1989).
- P. H. Ballentine, A. M. Kadin, M. A. Fisher, D. S. Mallory, and W. R. Donaldson, "Microlithography of High-Temperature Superconducting Films: Laser Ablation vs. Wet Etching," *IEEE Trans. Magn.* **25**, 950-953 (1989).
- P. Maine and G. Mourou, "Amplification of 1-nsec Pulses in Nd:Glass Followed by Compression to 1 psec," *Opt. Lett.* **13**, 467-469 (1988).
- E. M. Epperlein, G. J. Rickard, and A. R. Bell, "A Code for the Solution of the Vlasov-Fokker-Planck Equation in 1-D or 2-D," *Comput. Phys. Commun.* **52**, 7-13 (1988).
- S. Skupsky and T. Kessler, "A Source of Hot Spots in Frequency-Tripled Laser Light," *Opt. Commun.* **70**, 123 (1989).
- P. C. Cheng, S. P. Newberry, H. G. Kim, and M. D. Wittman, "X-Ray Contact Microradiography and Shadow Projection X-Ray Microscopy," *Europ. J. Cell Biol. Suppl.* **25** **48**, 169-172 (1989).
- R. L. McCrory, J. M. Soures, C. Verdon, M. Richardson, P. Audebert, D. Bradley, J. Delettrez, L. Goldman, R. Hutchison, S. Jacobs, P. Jaanimagi, R. Keck, H. Kim, T. Kessler, J. Knauer, R. Kremens, S. Letzring, F. Marshall, P. McKenty, W. Seka, S. Skupsky, and B. Yaakobi, "High-Density Laser-Fusion Experiments at the Laboratory for Laser Energetics," *Laser Interaction and Related Plasma Phenomena*, edited by H. Hora and G. H. Miley (Plenum Press, New York and London, 1989), pp. 483-502.
- M. C. Richardson, D. K. Bradley, P. A. Jaanimagi, J. Delettrez, R. Epstein, C. F. Hooper, R. C. Mancini, and D. Kilcrease, "X-Ray Diagnosis of High-Density Compression of Ar-Filled Polymer Shell Targets," *Rev. Sci. Instrum.* **59**, 1851 (1988).

## **Forthcoming Publications**

- R. L. McCrory and C. P. Verdon, "Computer Modeling and Simulation in ICF," to be published in *Il Nuovo Cimento*.

W. R. Donaldson, "Radial Line Structure Experiments," to be published in the *Proceedings of the 4th Workshop: Pulse Power Techniques for Future Accelerators*, Erice, Sicily, 3–10 March 1988.

G. Mourou, "Picosecond Electro-Optic Sampling," to be published in the *Proceedings of the High Speed Electronics Conference*, Stockholm, Sweden, August 1986.

R. L. McCrory and J. M. Soures, "Inertially Confined Fusion," to be published in *Applications of Laser Plasmas*, Chapter 7.

G. J. Rickard, A. R. Bell, and E. M. Epperlein, "2-D Fokker-Planck Simulations of Short Pulse Laser-Plasma Interactions," to be published in *Physical Review Letters*.

J. M. Soures, "Remarks of J. M. Soures at the Fusion Power Associates Panel Discussion," to be published in the *Journal of Fusion Energy*.

R. L. McCrory, J. M. Soures, C. P. Verdon, S. Skupsky, T. J. Kessler, S. A. Letzring, W. Seka, R. S. Craxton, R. Short, P. A. Jaanimagi, M. Skeldon, D. K. Bradley, J. Delettrez, R. L. Keck, H. Kim, J. P. Knauer, R. L. Kremens, and F. J. Marshall, "Laser Compression and Stability in Inertial Confinement Fusion," to be published in the *Proceedings of the 16th European Conference on Controlled Fusion and Plasma Physics*, Venice, Italy, 13–17 March 1989.

W. R. Donaldson, A. M. Kadin, P. H. Ballentine, and R. Sobolewski, "Interaction of Picosecond Optical Pulses with High-Tc Superconducting Films," to be published in *Applied Physics Letters*.

A. Simon and R. W. Short, "Comments on 'Studies of Raman Scattering from Overdense Targets Irradiated by Several Kilojoules of 0.53- $\mu\text{m}$  Laser Light'," to be published in *Physics of Fluids*.

A. Simon and R. W. Short, "Energy and Nonlinearity Considerations for the Enhanced Plasma Wave Model of Raman Scattering," to be published in *Physics of Fluids*.

J. Nees, S. Williamson, and G. Mourou, "100-GHz Traveling-Wave Electro-Optic Phase Modulator," to be published in *Applied Physics Letters*.

T. B. Norris, N. Vodjdani, B. Vinter, C. Weisbuch, and G. A. Mourou, "Time-Resolved Observation of Luminescence from a Charge-Transfer State in Double Quantum Wells," to be published in the *Proceedings of Quantum Wells for Optics and Optoelectronics Conference*, Salt Lake City, UT, 6–8 March 1989.

T. B. Norris, X. J. Song, G. Wicks, W. J. Schaff, L. F. Eastman, and G. A. Mourou, "Electric Field Dependence of the Tunneling Escape Time of Electrons from a Quantum Well," to be published in the *Proceedings of the Picosecond Electronics and Optoelectronics Conference*, Salt Lake City, UT, 8–10 March 1989.

M. Pessot and G. Mourou, "Chirped Pulse Amplification of 100 fs Pulses," to be published in *Optics Letters*.

P. C. Cheng and H. G. Kim, "The Use of X-Ray Contact Micro-radiography in the Study of Silica Deposition in the Leaf Blade of *Zea*

*mays L.*," to be published in the *Maize Genetics Cooperation News Letter*, Department of Agronomy and US Department of Agriculture.

D. L. Smith, J. H. Kelly, and M. J. Shoup, "A Low Cost Active-Active Oscillator Utilizing Loss Feedback Control," to be published in *Applied Optics*.

J. C. Lambropoulos, "Analysis of Thermal Stress, Fracture and Strengthening by Ion Exchange in Glass for High Average Power Laser Applications," to be published in the *Journal of Applied Physics*.

M. L. Tsai, S. H. Chen, and S. D. Jacobs, "Optical Notch Filter Using Thermotropic Liquid Crystalline Polymers," to be published in *Applied Physics Letters*.

X. Zhou and T. Y. Hsiang, "Monte Carlo Study of Photo-Generated Carrier Transport in GaAs Surface Space Charge Fields," to be published in the *Journal of Applied Physics*.

L. DaSilva, A. Ng, B. K. Godwal, G. Chiu, F. Collet, M. C. Richardson, P. A. Jaanimagi, and Y. T. Loe, "Shock-Induced Shifts in the Aluminum K-Photoabsorption Edge," to be published in the *Physical Review Letters*.

Y. F. Maa and S. H. Chen, "Synthesis of Thermotropic Liquid Crystalline Side-Chain Polymers via Chemical Modification of Polymeric Carboxylic Acids," to be published in *Macromolecules*.

M. L. Tsai, S. H. Chen, K. L. Marshall, and S. D. Jacobs, "Thermotropic and Optical Properties of Chiral Nematic Polymers," to be published in *International Journal of Thermophysics*.

## Conference Presentations

R. L. McCrory, "A Critical Scientific Review of ICF," presented at the American Association for the Advancement of Science Annual Meeting, San Francisco, CA, 14-19 January 1989. (Presented by C. Verdon.)

---

The following presentations were made at the SPIE's O-E/LASE 1989 Conference, Los Angeles, CA, 15-20 January 1989:

T. Kessler, S. Skupsky, R. S. Craxton, S. Letzring, R. Short, M. Skeldon, and J. M. Soures, "Elements of Beam Smoothing for the High-Power Solid-State Laser."

J. H. Kelly, M. J. Shoup III, and D. L. Smith, "OMEGA Upgrade Staging Options."

M. D. Perry, E. M. Campbell, J. T. Hunt, F. Patterson, G. Mourou, P. Bado, and P. Maine, "Ultra-High Brightness Laser Project at LLNL."

---

The following presentations were made at the Picosecond Electronics Conference, Salt Lake City, UT, 6-10 March 1989:

T. B. Norris, X. J. Song, G. Wicks, W. J. Schaff, L. F. Eastman, and G. A. Mourou, "Electric Field Dependence of the Tunneling Escape Time of Electrons from a Quantum Well."

T. B. Norris, N. Vodjdani, B. Vinter, C. Weisbuch, and G. A. Mourou, "Time-Resolved Observation of Luminescence from a Charge-Transfer State in Double Quantum Wells."

F. W. Smith, H. Q. Le, V. Diadiuk, M. A. Hollis, A. R. Calawa, S. Gupta, M. Frankel, D. R. Dykaar, G. A. Mourou, and T. Y. Hsiang, "Picosecond GaAs Based Photoconductive Optoelectronic Detectors."

---

P. C. Cheng, V. H. Chen, H. G. Kim, and R. E. Pearson, "A Real-Time EPI-Fluorescent Confocal Microscope," presented at the 1st International Conference on Confocal Microscopy and 2nd International Conference on 3-D Image Processing in Microscopy, Amsterdam, The Netherlands, 15-17 March 1989.

#### ACKNOWLEDGMENT

The work described in this volume includes current research at the Laboratory for Laser Energetics, which is supported by Empire State Electric Energy Research Corporation, New York State Energy Research and Development Authority, Ontario Hydro, the University of Rochester, and the U.S. Department of Energy Office of Inertial Fusion under agreement No. DE-FC03-85DP40200.